

SPUTTER COATING ATOMIC FORCE MICROSCOPE  
CANTILEVERS FOR VARIOUS RESEARCH  
APPLICATIONS

THESIS

Presented to the Graduate Council of  
Southwest Texas State University in  
Partial Fulfillment of the Requirements

For the Degree

Master of SCIENCE

By

Kevin P. Wiederhold, B.S.

San Marcos, Texas  
December 2000

**COPYRIGHT**

**by**

**Kevin Paul Wiederhold**

**2000**

I would like to dedicate this thesis to all of my friends who have given me support and guidance through the years, to all of my family members who's love and confidence have driven me to achieve many wonderful goals in my life, and most of all, to my beautiful wife Lezlie who has given me the inspiration to succeed in life and excel in my studies.

## **ACKNOWLEDGEMENTS**

I would like to thank my advisor, Dr. Heather Galloway, for allowing me the experience to work in her lab, and for giving me the guidance and support to help me achieve my goals and excel in my studies both as an undergraduate and graduate student.

I would like to thank my thesis committee members, Dr. Michalk and Dr. Geerts, for the time and effort spent reviewing my work and for providing me with their insight and feedback. I would also like to thank the rest of my physics professors for their encouragement and guidance in my studies. I would like to give special thanks to Dr. Gutierrez for his contribution and support in my research.

To all of my family and friends I would like to give thanks for their never-ending support and overwhelming confidence in my work. I would like to give a very special thanks to my wonderful wife, Lezlie, for always standing by me whenever and wherever I needed her. Without her love and devotion I would not be where I am today.

December 12, 2000

# TABLE OF CONTENTS

	<b>Page</b>
LIST OF TABLES .....	viii
LIST OF FIGURES .....	ix
ABSTRACT .....	x
<b>Chapter 1</b>	
<b>Research Applications of Atomic Force Microscopy</b> .....	1
1.1 INTRODUCTION .....	1
1.1.1 ATOMIC FORCE MICROSCOPY .....	1
1.1.2 BASIC COMPONENTS AND OPERATION OF AFM .....	2
1.1.3 RESEARCH APPLICATIONS .....	4
1.2 CAPACITANCE IMAGING .....	5
1.2.1 AFM CAPACITANCE IMAGING .....	5
1.2.2 RESEARCH USES FOR CAPACITANCE IMAGING .....	6
1.2.3 HOW IT WORKS .....	8
1.3 CMP MODELING .....	10
1.3.1 INTRODUCTION TO CHEMICAL MECHANICAL PLANARIZATION .....	10
1.3.2 CMP MODELING WITH THE AFM .....	13
<b>Chapter 2</b>	
<b>Thin Film Selection</b> .....	16
2.1 MATERIAL SELECTION FACTORS .....	16
2.1.1 FILM ADHESION AND TIP GEOMETRY .....	16
2.1.2 DEPOSITION FACTORS .....	17
2.1.3 OTHER FACTORS .....	17
2.2 TITANIUM NITRIDE .....	18
2.2.1 FACTORS FOR CAPACITANCE IMAGING CANTILEVERS .....	18
2.2.2 WHY TITANIUM NITRIDE? .....	18
2.3 ALUMINUM OXIDE .....	19
2.3.1 FACTORS CONCERNING CMP MODELING CANTILEVERS .....	19
2.3.2 WHY ALUMINUM OXIDE? .....	20
2.4 FILM GROWTH .....	20
2.4.1 DEPOSITION METHOD .....	20
<b>Chapter 3</b>	
<b>DC Magnetron Sputtering</b> .....	22
3.1 DIRECT CURRENT MAGNETRON SPUTTERING .....	22

3.1.1	INTRODUCTION TO SPUTTERING.....	22
3.1.2	FUNDAMENTAL SPUTTERING PHYSICS.....	23
3.1.3	CONTROL OF REACTIVE AND NON-REACTIVE GAS FLOW..	26
3.1.4	DEPOSITION OF NON-CONDUCTIVE FILMS .....	27
3.1.5	PULSED MODE SPUTTER DEPOSITION.....	27
3.2	SUBSTRATE MOUNTING.....	30
3.2.1	CANTILEVER CHIP HOLDER FOR SPUTTERING SYSTEM ....	30
3.2.2	MATERIAL SELECTION FOR CANTILEVER HOLDER.....	31
3.2.3	CANTILEVER HOLDER DESIGN .....	32
3.2.4	SHUTTERS.....	33
<b>Chapter 4</b>		
<b>Experimental Results and Modifications</b> .....		36
4.1	EQUIPMENT CALIBRATION.....	36
4.1.1	CALIBRATION FILMS .....	36
4.2	PRELIMINARY RESULTS .....	37
4.2.1	ANALYSIS OF CALIBRATION FILMS .....	37
4.2.2	SPUTTER COATING AFM CANTILEVERS.....	37
4.2.3	APPLICATION TESTING FOR LASER ALIGNMENT .....	38
4.3	EXPERIMENTAL MODIFICATIONS .....	40
4.3.1	INTERFACIAL STRESS OF TITANIUM NITRIDE FILMS.....	40
4.3.2	TITANIUM SEED LAYER.....	40
4.3.3	DUAL TITANIUM TARGETS .....	41
<b>Chapter 5</b>		
<b>Film Analysis</b> .....		42
5.1	DEPOSITION RATES .....	42
5.1.1	FILM THICKNESS .....	42
5.1.2	TITANIUM/TITANIUM NITRIDE DEPOSITION RATES.....	44
5.1.3	ALUMINUM/ALUMINA DEPOSITION RATES.....	46
5.2	RESISTIVITY .....	47
5.2.1	FOUR-POINT-PROBE MEASUREMENTS.....	47
5.3	FILM UNIFORMITY AND ELEMENTAL ANALYSIS.....	51
5.3.1	SEM AND EDS MAPPING .....	51
5.4	ELECTRICAL PROPERTIES OF TITANIUM NITRIDE.....	52
5.4.1	CONDUCTIVITY .....	52
<b>Chapter 6</b>		
<b>Conclusions</b> .....		54
6.1	CONCLUSIONS .....	54
APPENDIX.....		56
BIBLIOGRAPHY .....		66

## LIST OF TABLES

Table 1 - List of sputtering parameters for calibration films. ....	36
Table 2 – Film thickness and calculated resistivities. ....	37
Table 3 – Deposition rates of various nitrogen gas flows. ....	44
Table 4 - Mean deposition rates and standard deviation. ....	45
Table 5 - Alumina deposition rates for different oxygen flows. ....	46
Table 6 - Dimensions and resistivity of several titanium nitride thin films. ....	48
Table 7 - Dimensions and resistivity for aluminum oxide thin films. ....	49

## LIST OF FIGURES

Figure 1 – Typical AFM components and setup. ....	3
Figure 2 – Simple transistor diagram. The yellow regions represent the dielectric material.....	6
Figure 3 - Capacitance imaging model with TiN coated cantilever. The AC signal is applied using a function generator and a lock-in amplifier monitors the second harmonic. ....	8
Figure 4 - Equipment setup for capacitance imaging.....	9
Figure 5 - CMP modeling with atomic force microscope.....	14
Figure 6 – Thin film coverage of AFM tip geometry. ....	17
Figure 7 - Sputter target/magnet assembly w/ field lines. ....	24
Figure 8 - Sputter chamber showing guns, targets, and shield.....	25
Figure 9 - Schematic of mass flow controllers and gas flow. ....	26
Figure 10 - Schematic of Sparc-le 20 (courtesy of Advanced Energy) ....	28
Figure 11 - (courtesy of Advanced Energy) .....	30
Figure 12 - Size comparison of AFM cantilever chip. ....	31
Figure 13 - Diagram of cantilever holder. ....	32
Figure 14 - Dimensions of cantilever holder channels. ....	33
Figure 15 - Top view of shutter. ....	34
Figure 16 – Cross-sectional view of cantilever chip mounted in holder. ....	35
Figure 17 - Proper laser alignment on cantilever.....	38
Figure 18 - Improper laser alignment.....	39
Figure 19 - Position of mask mounted on substrate during sputtering process. ....	42
Figure 20 – Step of sputtered material after mask removal.....	43
Figure 21 – EDS mapping of SEM image of AFM Ultralever. ....	51
Figure 22 – (I vs. V) plot of coated and uncoated AFM Ultralever. ....	53

## **ABSTRACT**

### **SPUTTER COATING ATOMIC FORCE MICROSCOPE CANTILEVERS FOR VARIOUS RESEARCH APPLICATIONS**

by

**KEVIN PAUL WIEDERHOLD, (B.S.)  
Southwest Texas State University  
December 2000**

**SUPERVISING PROFESSOR: HEATHER GALLOWAY**

The atomic force microscope is used in a variety of ways to examine the atomic-scale physical properties of materials. We have used our AFM for capacitance imaging and chemical mechanical planarization (CMP) modeling. Capacitance imaging allows us to effectively image the local dielectric properties of materials. By modeling atomic scale CMP mechanisms we can gain insight to some of the “black-art” of this science. Operating this instrument in these ways requires the use of specialized cantilever tips. For our capacitance imaging we fabricated a tip that is both durable and conductive by coating the standard silicon oxide AFM cantilevers with titanium nitride. Cantilevers were also fabricated for our atomic-scale CMP modeling application using certain specialized materials such as aluminum oxide. These coated tips were fabricated using our DC Magnetron Sputtering System. After the cantilever chips were coated, they were analyzed in order to determine their physical properties. From this research we have shown that is possible for small research groups to effectively and cost-consciously sputter-coat microfabricated AFM cantilevers for specific research applications.

## **CHAPTER 1**

### **Research Applications of Atomic Force Microscopy**

#### **1.1 INTRODUCTION**

##### *1.1.1 ATOMIC FORCE MICROSCOPY*

The atomic force microscope (AFM), which was developed in the mid 1980's, enabled scientists to measure a physical quantity with atomic scale resolution. This new quantity, with atomic-scale resolution, was the force between a small tip and a surface. Unlike its predecessor, the scanning tunneling microscope (STM), the AFM could image non-conductive surfaces. This meant that insulators and semiconductors could be analyzed at the atomic scale. The AFM is a vitally important instrument used for materials research. This instrument can be used in a variety of ways to examine the atomic-scale physical properties of materials. Unlike traditional microscopes, the AFM does not use lenses, so the size of the probe and the distance between the probe and the sample rather than diffraction effects generally limits its resolution. Atomic force microscopes can achieve a resolution of about 10 pm in the z-direction, and unlike electron microscopes, can image samples in air and under liquids.<sup>1-3</sup>

### *1.1.2 BASIC COMPONENTS AND OPERATION OF AFM*

Although it is a recent addition to the science/technology world, the atomic force microscope is best described as similar to an old record player. The tip is held above the surface to be scanned by a spring lever with a spring constant that is known to an order of magnitude. It has been a common practice to use the displacement of springs as a measurement of force. Previous methods have relied on electrostatic fields, magnetostatic fields, optical waves and x rays.<sup>4</sup> The sample below sits on a piezo tube that moves the sample back and forth under the tip, similar to a record moving under the needle of a record player. In many cases, scanning is done with the tip and sample in contact. A laser is deflected off the back of the tip to a position sensitive photo-detector (PSPD). The laser deflections are detected by the PSPD and the data is sent to the computer for processing. Once the computer receives the data it can also control the motion of the piezo scanner via a feedback loop. The computer creates a software-rendered image of the data collected from the cantilever deflections. The following figure represents the basic components of a typical atomic force microscope.

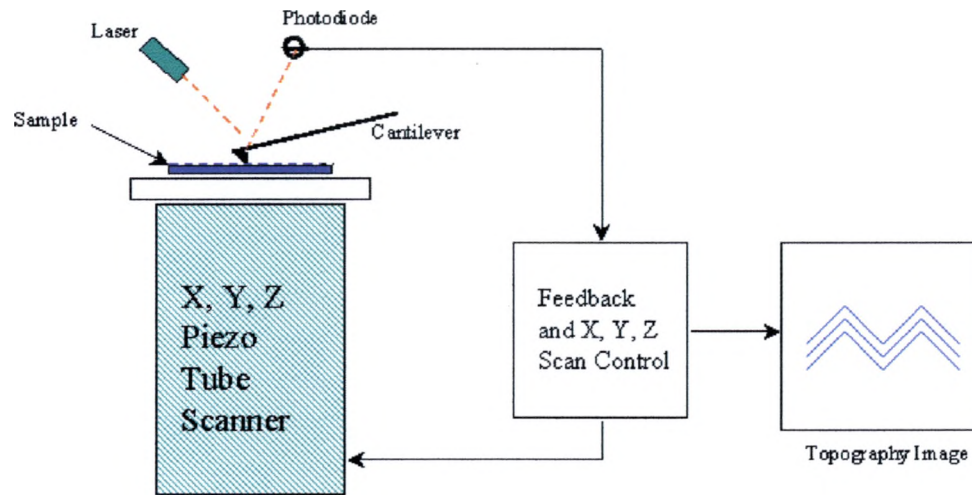


**Figure 1 – Typical AFM components and setup.**

The photodiodes on our AFM are partitioned into two or four quadrants depending on the type of image needed. The four-quadrant photodiode is used primarily for lateral force imaging while the two-quadrant PSPD is often used for normal imaging. The two quadrants can be thought of as an A-side and a B-side. When positioning the laser on the photodiode it is desirable to have the intensity of the sum of both sides ( $A+B$ ) at a maximum. This ensures the entire deflected laser is on the detector. The magnitude of difference of the two sides ( $A-B$ ) should be kept to a minimum, or as close to zero as possible. This helps to ensure the laser is centered on the PSPD and allows for maximum range of motion. Since we are essentially measuring the variations of the laser from its centered position, we generally think of the signal coming from the PSPD as the ( $A-B$ ) signal. The computer and software receive this

signal and adjust the height of the piezo scanner via a feedback loop to keep the signal constant. The amount of piezo movement is used to determine the sample displacement, which is used to create the software rendered image on the screen.

### *1.1.3 RESEARCH APPLICATIONS*

The atomic force microscope is widely used in the semiconductor microelectronics industry as a tool for profiling the surface of thin film oxides and nitrides as well as many other surfaces.<sup>5</sup> The AFM can be adapted and used for capacitance imaging of dielectric materials and for chemical mechanical planarization (CMP) modeling. Both of these uses of the AFM require advanced imaging techniques and instrument modification. We have adapted our AFM, a Park Scientific *AUTOPROBE CP*, to meet our research imaging requirements. In both cases microfabricated cantilevers are coated with case-specific materials to enhance imaging performance. Titanium nitride is used to coat the capacitance imaging cantilevers since this material is both conductive and durable. Aluminum oxide is used to coat the CMP modeling cantilevers to stimulate the abrasive alumina particles required for the process.

## **1.2 CAPACITANCE IMAGING**

### *1.2.1 AFM CAPACITANCE IMAGING*

The AFM is a very powerful tool in the materials science/semiconductor industry today used to investigate electronic characteristics of surfaces on a submicron scale.<sup>6</sup> Its ability to image atomic scale surface features makes it extremely useful for imaging the local dielectric properties of materials. By applying a bias between the AFM tip and the sample the electrostatic forces acting on them can be measured. The capacitance imaging techniques of the Atomic Force Microscope enable us to learn much about the local dielectric properties of insulated materials. While imaging the dielectric properties of the samples it is necessary to have uniformity in the scan images. Degradation of the tip is one of the main problems that inhibits uniform scans of the sample. Since the atomic force microscope relies upon tip-sample interaction, and since there is material deterioration associated with such interactions, it is desirable to have a wear resistant imaging tip. For capacitance imaging a tip is needed that is both durable and conductive. In order to decrease the rate of tip degradation and increase the uniformity in the scan images it is desirable to coat the relatively soft silicon tip with a hard, conductive material. To reduce the degree to which this factor affects the AFM image the tips used for capacitance imaging can be coated with a metallic TiN thin film.<sup>7-9</sup>

### 1.2.2 RESEARCH USES FOR CAPACITANCE IMAGING

High-k dielectric research is one of the main reasons that we are interested in the capacitance measurements of our samples. With the current trend in technology, a primary goal is creating smaller and faster electronic devices. In order to accomplish these goals it is necessary to construct smaller transistors for use in integrated circuits. One of the limiting factors in the size of the transistors in the IC is the dielectric constant of the gate dielectric material. The figure below is a simple drawing that can be used to explain the transistor limitations.

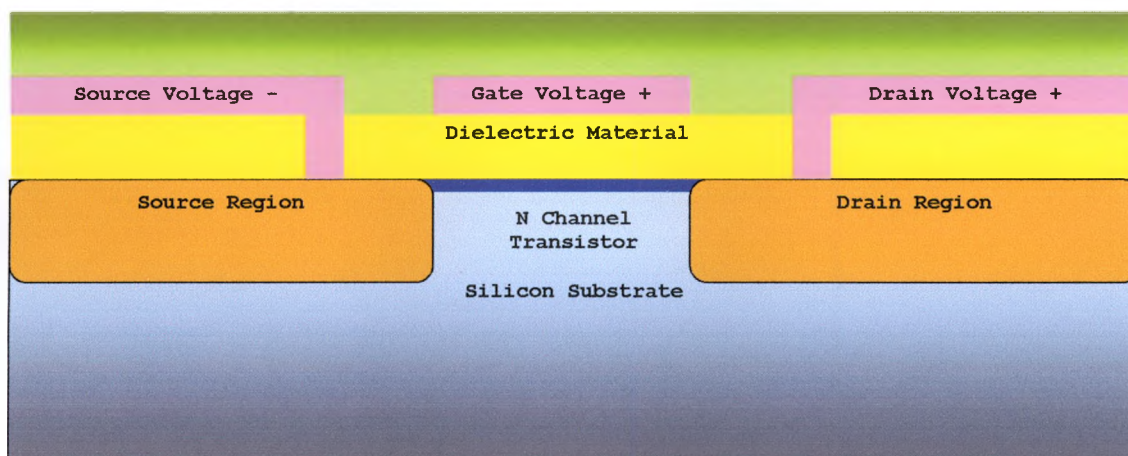


**Figure 2 – Simple transistor diagram. The yellow regions represent the dielectric material.**

As you can see from this model of a transistor the dielectric material isolates the gate, source, and drain electrodes. Isolation of these regions of the transistor is essential to prohibit device failure. In order to decrease the size of the transistor on the integrated circuit you need to decrease the size of its features. High-k dielectric materials are

also used for storage capacitors in memory devices such as RAM chips. The equation describing the capacitance of simple parallel plate capacitor is:

$$C = k\epsilon_0 A/d$$

For this equation,  $k$  is the dielectric constant of the insulating material between the plates,  $A$  is the surface area of the plates,  $d$  is the distance between the plates, and  $\epsilon_0$  is the permittivity constant.

The region of the transistor between the gate electrode and the substrate behaves in a fashion similar to the parallel plate capacitor. One way to decrease the size of the transistor is to minimize  $d$ , or the distance between the capacitive plates on the transistor. However, this distance is also limited by a minimal distance at which electrons begin to tunnel across the barrier causing a leakage current. The leakage through the dielectric increases exponentially with the decrease in the material thickness. This leakage current causes the device to fail. Therefore, in order to make the device smaller, while at the same time increasing the capacitance (to prevent leakage current) a material with a higher dielectric constant must be used. The surface of the plates would also affect the capacitance but since we want to decrease the overall size of the device it is not possible to increase the surface area of the plate without making complicated structures that increase process cost.

These electrical properties of the simple transistor in integrated circuits are the reason we are interested in the local dielectric properties of the materials we are imaging. By using the AFM for capacitance imaging it is possible to analyze how the electrical properties of the sample change across its surface. In this way we are able to analyze different materials used in the semiconductor industry and inspect them for defects. The figure below illustrates how the TiN coating on the cantilever tip is used to enhance our imaging methods.

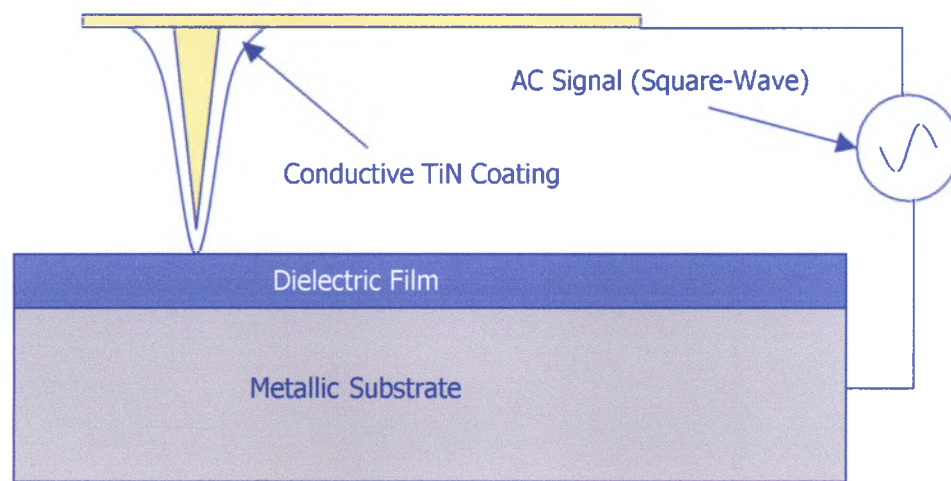


**Figure 3 - Capacitance imaging model with TiN coated cantilever. The AC signal is applied using a function generator and a lock-in amplifier monitors the second harmonic.**

### 1.2.3 HOW IT WORKS

In capacitance mode the Atomic Force Microscope operates in topographic scan setup that utilizes the instruments feedback loop and (A-B) signal to acquire images of the topography and capacitance of the sample simultaneously. In conjunction with the regular topography

setup, a lock-in amplifier is also used as well as an AC bias source. The basic configuration of this setup is illustrated in figure 4.

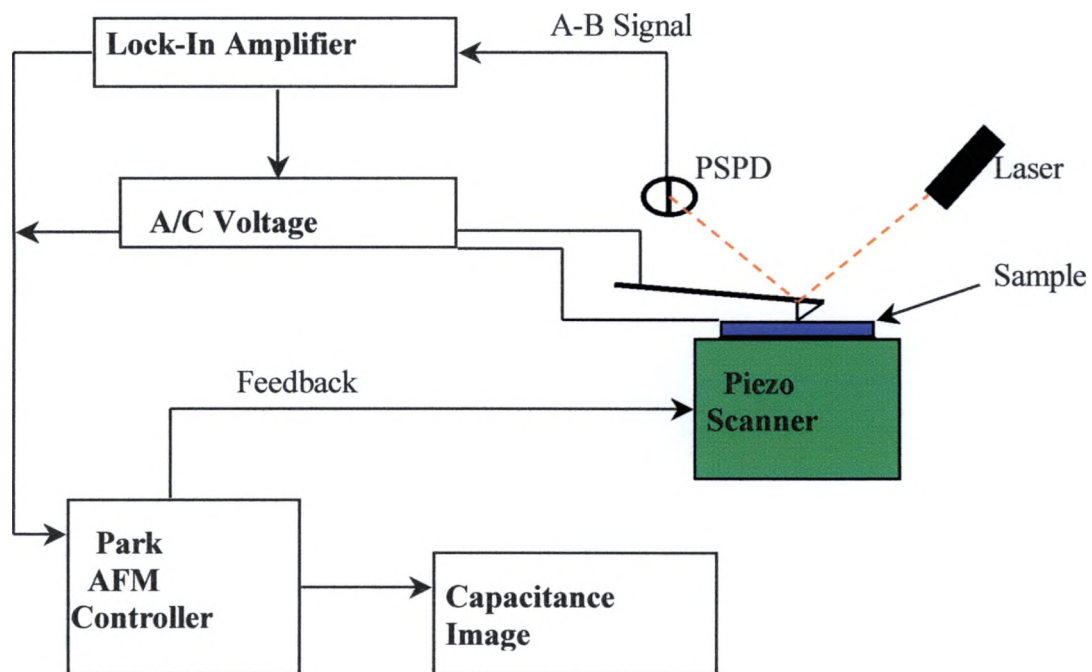


**Figure 4 - Equipment setup for capacitance imaging.**

The lock-in amplifier in the arrangement is used to extract a certain frequency ( $2f$ ) from the A-B signal sent by the photosensitive photodiode (PSPD). The bias between the tip and the sample surface is applied at or near the resonance frequency of the tip ( $f$ ). This causes the tip to vibrate at the surface of the sample and enables it to sense minute changes in the electrical properties of the sample surface (i.e. capacitance). The ( $2f$ ) signal is captured by the lock-in since the capacitive force between the tip and sample is proportional to twice the

resonance frequency of the cantilever. Thus, when the cantilever is oscillated at this frequency, the A-B signal carries the signal frequency describing the capacitance force felt by the tip. The (A-B) signal is sent to the lock-in and then transferred to the electronics and feedback loop allowing the computer software to render the images of both the topography and the capacitance force.<sup>2,10</sup>

The resolution of the acquired images depends mainly on the shape and condition of the tip. The condition of the AFM tip is very important while capacitance imaging. The AFM Ultralevers that we generally use are silicon based. These tips tend to wear fast under the strains of the capacitance setup. A close look at some images reveals a noticeable degradation of the tip during a single scan. One way to combat this problem of tip erosion is to coat the Ultralevers with a hard thin film such as titanium nitride. The thin film also must not have a surface oxide or be a semiconductor since we want to apply a bias between the tip and sample. Titanium nitride is also suitable for these requirements.

## **1.3 CMP MODELING**

### *1.3.1 INTRODUCTION TO CHEMICAL MECHANICAL PLANARIZATION*

Today's high performance circuits contain many areas with a high density of tall and narrow features. These features produce dense, high aspect ratio topography on the surface of the integrated circuit. When

this topography exists on an inter-level dielectric film deposited over one level of metal, it makes it nearly impossible to directly deposit the next metal layer. There are two reasons for this: First, the step coverage of interconnect metallization films deposited over this topography will be very poor. This will result in thinned areas of interconnect lines. These areas can form local hot spots and possibly cause higher electro-migration liability. Secondly, lithography on a film deposited on this severe topography will also be very poor since the depth of focus of the high NA lenses needed for sub 0.5  $\mu\text{m}$  feature patterning is smaller than the feature height. The result would be that the patterns would be in focus only at one depth. This means that the patterns can be focused on the top of the features, the middle of the features, or the bottom of the features. The remainder of the patterned lines would be out of focus and therefore broadened relative to the desired feature width.<sup>11</sup>

To combat these problems the wafer is put into a chemical mechanical planarization process after inter-level dielectric deposition and the dielectric is polished until its surface is flat. Even though the dielectric over the metal is thinner than between metal lines, enough is deposited before polishing that a layer of sufficient thickness is left. The next metal layer can then be deposited onto a flattened surface and the process repeated until the final metal layer is put down. These planarized metal layers are much more reliable than metal layers which have been deposited over significant topography.<sup>11</sup>

The CMP process involves putting the wafer in a polishing station on a revolving platen and polishing it with a rotating pad with a slurry flowing around and through the brush. The slurry is generally a suspension of colloidal silica in a pH-controlled liquid for polishing dielectrics such as TEOS, or colloidal alumina suspended in a pH-controlled liquid for polishing tungsten. The polishing process is a combination of grinding of the surface by the 'grit' and chemical passivation/removal. This mechanical action in such a chemical environment gives rise to the name chemical mechanical planarization.

Removal rates by this process can be very high but, unfortunately, quite variable since they depend on many parameters. The rotation rate of the pad, rotation rate of the wafer, flow rate of the slurry, pressure of the pad against the wafer, and pH or chemical activity of the slurry are all controlling factors in the overall polishing rate for the wafer. Less obvious parameters are the interconnect pattern density, pitch, area, and geometric aspect ratio. All of these parameters interact with the polishing process parameters and cause variations in removal rate across the individual die. These local variations are repeated across the wafer and are in some sense convoluted with the small variations in pressure between the center, middle, and edge regions of the wafer. This produces wide variations in local removal rate.<sup>11</sup>

CMP processes have been used for over 30 years to prepare silicon wafers for IC manufacturing. More recently, however, this process has

been adapted in many microelectronics fabs for polishing metal for tungsten plug formation and embedded metal structures. CMP of metals involves hard particles suspended in aqueous solutions (slurries). The slurry interacts with the metal surface because of the mechanical force applied by the polishing pad. This particle/metal interaction can be simulated through the interaction between the tip and sample of an atomic force microscope. By modeling atomic scale CMP mechanisms we can gain insight to some of the “black-art” of this science.

### *1.3.2 CMP MODELING WITH THE AFM*

The AFM is being used to solve process and material problems in a wide number of technological industries. These industries include electronics, telecommunications, biomedical, chemical, automotive, aerospace, and energy industries.<sup>12</sup> It has been shown that the particle/metal interaction of the CMP process can be simulated by the interaction of an AFM tip with a sample surface. Characterization of surface topography by AFM is typically performed under conditions that minimize tip/sample interaction. However, in order to simulate the CMP process, the opposite conditions are desired.<sup>13</sup> Our goal was to coat the AFM tips with alumina and image our tungsten samples while they were submerged in a chemical bath representative of a slurry of known effectiveness. For our research, one of the slurries investigated consisted of a peroxide solution with suspended abrasive alumina particles. The

$\text{Al}_2\text{O}_3$  coating on the atomic force microscope cantilevers allows the tip apex to mimic the role of the  $\text{Al}_2\text{O}_3$  particles in the CMP slurry. Using the cantilever tips, we are able to model the atomic-scale mechanisms of the CMP process. By scratching our coated tips on the tungsten in solution we hope to mimic the atomic scale CMP mechanisms driving the removal of material. The figure below represents the basic CMP mechanisms performed by the AFM.

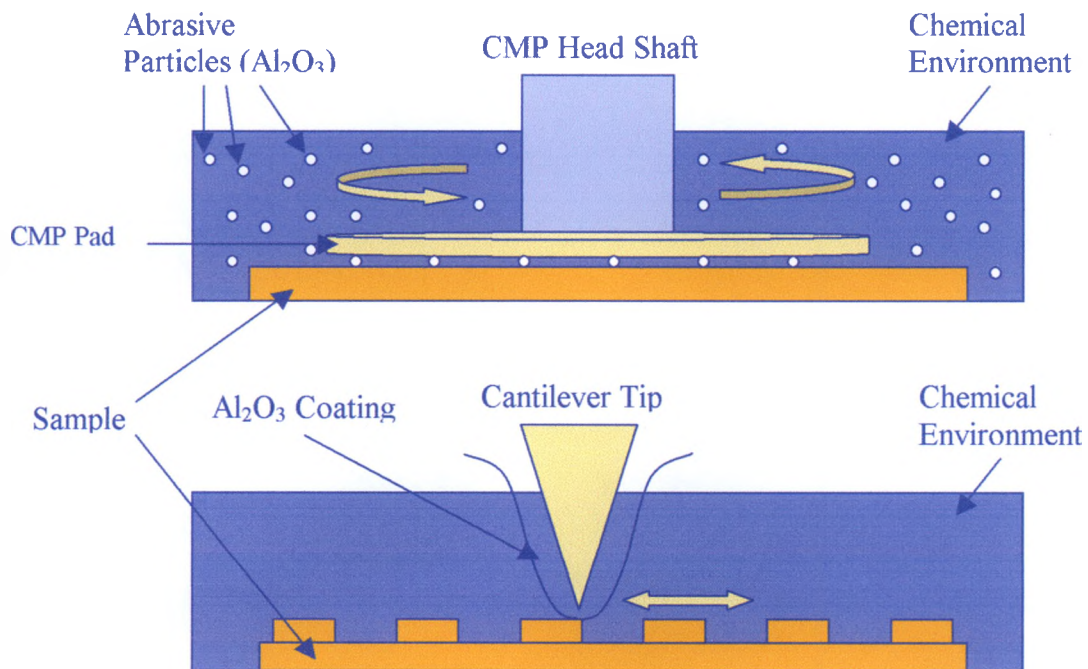


**Figure 5 - CMP modeling with atomic force microscope.**

This diagram shows how the mechanical motion of the polishing pad is replaced by the scanning of the sample beneath the AFM tip. It

also illustrates how coating the AFM tip with alumina serves to localize the effects of the CMP process on the surface of the sample.

## **CHAPTER 2**

### **Thin Film Selection**

#### **2.1 MATERIAL SELECTION FACTORS**

##### *2.1.1 FILM ADHESION AND TIP GEOMETRY*

There are several factors to consider when selecting a material for thin film coating of atomic force microscope cantilevers. One factor that is important in the material selection for both types of imaging is the adhesion strength. The adhesion strength determines how well the thin film sticks to the substrate. It is one thing to deposit a relatively flat and uniform thin film on a thick, flat substrate. However, it is much more difficult to deposit a flat uniform film on a thin cantilever with high geometric features. Due to the geometry of the AFM tip, it is necessary to have proper film adhesion in order to ensure complete coverage of the tip area. It is extremely important to have total coverage of the tip apex where the tip/sample interaction is strongest. The following image is a representation of what the expected thin film coated cantilever profile would look like. The film coverage of the tip apex increases the radius of curvature of the tip. This drawing illustrates how the geometry of the cantilever tip can have a dramatic effect on the thickness and shape of the deposited thin film.

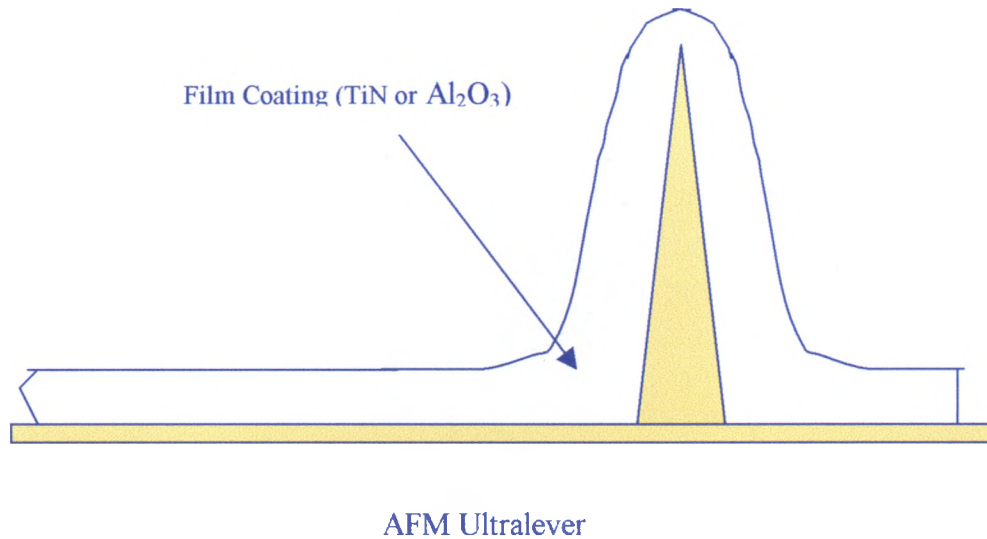


**Figure 6 - Thin film coverage of AFM tip geometry.**

### *2.1.2 DEPOSITION FACTORS*

When deciding on a thin film material we also considered the many deposition factors involved. The availability of material, cost of sputtering targets, and ease of sputter deposition were all important factors in determining which type of material was suitable for each application. For example, gold is an excellent conductor and was considered for the capacitance imaging tips. Gold is also easily sputtered using DC Magnetron Sputtering. However, it is also a relatively soft metal and the sputtering targets are very expensive.

### *2.1.3 OTHER FACTORS*

Other factors in the selection of material for tip coatings are more dependent on the different applications. Material strength, electrical

properties, and chemical reactivity are all considered when determining which material to use for the cantilever coatings. For the capacitance imaging tips, conductivity and film durability were key factors in the selection of titanium nitride for the thin film coatings. The tips used for CMP modeling needed to be aluminum oxide since they would be replacing the abrasive alumina particles in the slurry we selected.

## **2.2 TITANIUM NITRIDE**

### *2.2.1 FACTORS FOR CAPACITANCE IMAGING CANTILEVERS*

The cantilever tips used for capacitance imaging have to be conductive in order to allow a bias between them and the sample. These tips also need to be durable enough to repeatedly provide accurate images. For these reasons we considered several metallic thin films for cantilever coatings. There were several characteristics the metallic thin films needed to have in order to work properly. A metal with a relatively low resistivity was desirable in order to provide for the good conductance of the tip. Another characteristic we were looking for was the strength of the metal used to coat the tips.

### *2.2.2 WHY TITANIUM NITRIDE?*

There were several types of metal films that did not meet our requirements. Many elemental conductors tend to have a native oxide layer form on their surface. This oxidation can inhibit the conductive

properties of coated cantilevers. The metal film that we decided to use for the coatings was titanium nitride (TiN). TiN does not form a considerable native oxide on its surface. Titanium nitride also has a low resistivity and a high microhardness, which makes it ideal for our applications. This material is also widely used in industry today for a variety of purposes. <sup>14-16</sup> Its strength lends it to be a great drill bit and saw blade coating. It is also used as an artificial gold color on most imitation jewelry. The fact that it was readily available to us and that it will stick to almost anything are two more reasons that we chose TiN as our metal coating for the tips. The cost of the titanium targets was also much less than sputtering targets of other conductive metals such as gold or platinum. <sup>17,18</sup>

## **2.3 ALUMINUM OXIDE**

### *2.3.1 FACTORS CONCERNING CMP MODELING CANTILEVERS*

The requirements for the thin film coating used for our CMP modeling technique were more specific than for the capacitance imaging. Chemical mechanical planarization requires a chemical slurry along with the mechanical polishing action to work effectively. These slurries often include small abrasive particles that are required for effective planarization. There are several different slurries available for different types of polishing processes, depending on the material to be polished.

### *2.3.2 WHY ALUMINUM OXIDE?*

Two important materials for us to research were copper and tungsten. One slurry used for polishing both metals required small aluminum oxide (alumina) particles to complete the chemical reaction. Since our application is material specific we knew that we needed to use aluminum oxide to coat the cantilevers for this application. The tip-sample contact between our coated tips and the tungsten is used to replace the alumina particles in the slurry recipe. Since the only source of alumina particles is the cantilever tip we are able to localize the CMP process. By localizing the process we can effectively image atomic-scale CMP mechanisms.

## **2.4 FILM GROWTH**

### *2.4.1 DEPOSITION METHOD*

Once we decided on which materials we would use to coat our AFM cantilevers we had to determine a deposition method. The method we chose to use to deposit our thin films onto our cantilevers tips was magnetron sputtering. Sputtering has a number of widely recognized advantages over other deposition techniques that have led to its growing use. Sputtering thin films offers improved adhesion, improved stoichiometry, improved step coverage, and flexibility. The improved adhesion results from the kinetic energy of the sputtered atoms or molecules being orders of magnitude greater than other deposition

methods. The ease of depositing compounds and maintaining composition leads to the increased stoichiometry. Improved step coverage is achieved as a result of the increased kinetic energy and various angles of incident particles. The flexibility of the sputtering process lends itself to adaptation for complex research applications as well as high volume production uses. 19

## **CHAPTER 3**

### **DC Magnetron Sputtering**

#### **3.1 DIRECT CURRENT MAGNETRON SPUTTERING**

##### *3.1.1 INTRODUCTION TO SPUTTERING*

Sputtering as a method of film deposition has been known since at least 1852. This makes the process of sputtering comparable in age to the evaporation method.<sup>20</sup> Magnetron sputtering is a type of Physical Vapor Deposition (PVD) technique. As mentioned earlier, the equipment used to coat the tips was the DC Magnetron sputter deposition system. This system uses a reactive sputtering process to deposit the target material on the substrates. The substrates we were using were atomic force microscope cantilevers. These cantilevers are made of silicon and have an oxide layer on the surface. Titanium nitride and aluminum oxide were the two primary materials we used for the thin film deposition onto the AFM cantilevers with Ti or Al as adhesion layers. Titanium nitride is grown in a reactive sputtering process using a Ti target with nitrogen gas flow. Aluminum oxide is typically also grown in a reactive sputtering process using an aluminum target and in an oxygen atmosphere.<sup>18</sup>

### *3.1.2 FUNDAMENTAL SPUTTERING PHYSICS*

The reactive sputtering method utilizes a vacuum chamber filled with a non-reactive gas (argon) and a reactive gas (nitrogen or oxygen). Sputtering of target material is achieved by bombarding the target with energetic ions. In a sputter deposition process there are two primary sources of energetic particles incident at the substrate growing film. One of the sources is ions that are accelerated towards the target, neutralized, and reflected towards the substrate. The second source is ions that are accelerated toward the substrate by an applied or induced substrate bias. The second source is by far the dominant source. <sup>21</sup> These ions, which are present in the chamber due to the ionization of the inert argon gas, form a plasma ring in the chamber. A DC magnetron plasma is a magnetized glow discharge. This glow discharge is typically established between the cathode (target source) and the anode (substrate). The target material is eroded away by ions accelerated towards it due to its negative potential. A magnetic field is present in the chamber due to a magnet housed below the target material. This magnetic field serves as an electron trap that increases the ionization rate and sputtering efficiency. A diagram of the target/magnet assembly is given below. <sup>22</sup>

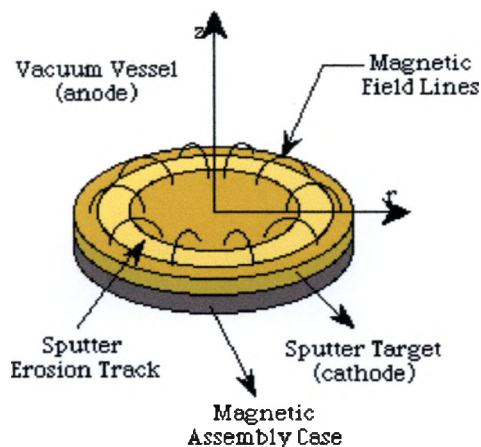


**Figure 7 - Sputter target/magnet assembly w/ field lines.**

In the DC Magnetron Sputtering system, the conductive Al or Ti targets act as the cathode in a diode system. Consequently, this type of deposition process will not work using targets made from non-conductive dielectric materials. The target sits in the center of the round cylinders pictured above. These targets sit on top of strong magnets that are above the “guns”. These “guns” are energized by a DC power supply and used to ignite the plasma, which is located just above the cathode. The magnetron guns are used to supply a negative potential and a strong magnetic field. The negative potential accelerates the argon ions towards the target material and the magnetic field is used to trap electrons in a helical circular path above the target. These accelerated ions move toward the target with energies of up to several hundred electron volts. Upon impacting, each incident particle starts a cascade of collisions near the surface of the target. These collisions may or may not result in the ejection of a sputtered target atom. As mentioned earlier, this plasma is

held in a torus (doughnut) shape above the target by the strong magnets beneath them. <sup>19,23</sup> A picture of the sputtering chamber is given below.



**Figure 8 - Sputter chamber showing guns, targets, and shield**

Above the targets are circular shutters that are kept in place to shield the substrates from sputtered material until they are ready to be sputtered. Centered above the shutters one can observe a rectangular object, which is used to hold the sample substrates (AFM tips). This holder also encloses a heater that can be used to heat the substrates while they are being sputtered. Controlling the temperature of the substrates during the sputtering process is an important parameter affecting the film quality. <sup>24</sup>

### 3.1.3 CONTROL OF REACTIVE AND NON-REACTIVE GAS FLOW

The flow of the argon gas mentioned above is controlled by Mass Flow Controllers (MFC) that are arranged just outside the sputtering chamber. These MFC's are connected to an electronic controller that regulates the amount of gas allowed to flow through the controllers. Mass flow controllers are used to regulate the flow of reactive and non-reactive gases into the chamber. The diagram below shows how the MFC's are arranged in a typical sputtering system.

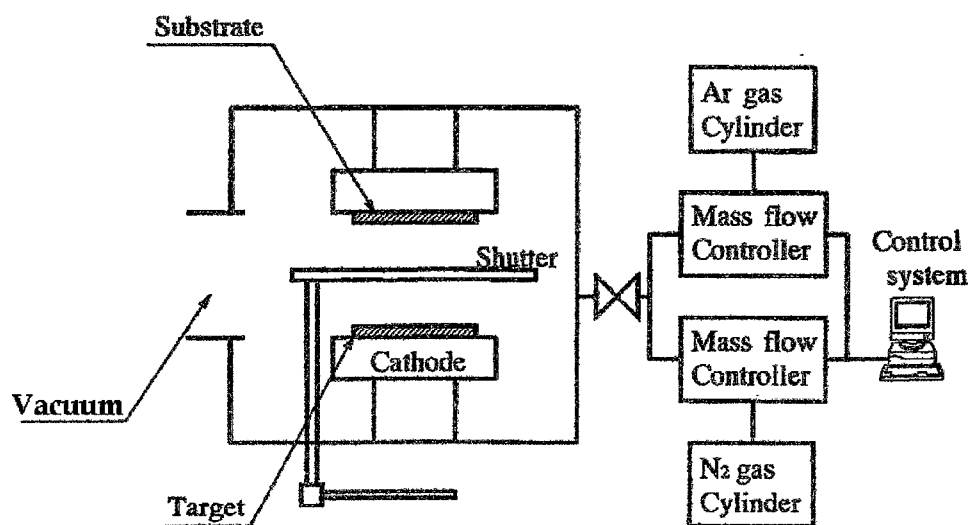


Figure 9 - Schematic of mass flow controllers and gas flow.

This illustration also shows how individual mass flow controllers are used for each type of gas flowing into the sputtering chamber. In this case, argon is the non-reactive gas and nitrogen is the reactive gas. However, when sputtering aluminum oxide for example, the reactive gas would be oxygen instead of nitrogen.

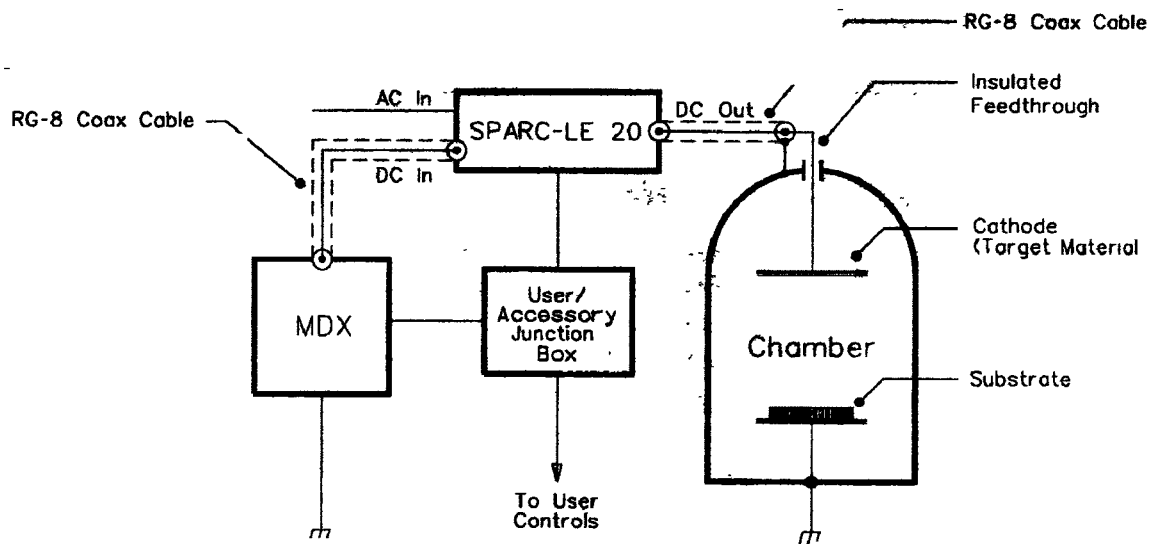
### *3.1.4 DEPOSITION OF NON-CONDUCTIVE FILMS*

Although sputtering with the DC Magnetron system usually requires a conductive target material to operate, it is possible to deposit non-conductive films with it. Oxide coatings can be produced by the reactive direct current sputtering of a metallic target in an oxygen atmosphere. <sup>25</sup> For example, when sputtering a dielectric such as aluminum oxide, a conductive elemental aluminum target can be used. Sputtering with this target, while flowing a reactive gas such as oxygen, allows for the deposition of alumina ( $\text{Al}_2\text{O}_3$ ). During the sputter deposition of alumina insulating material tends to build up on the target. The build up of an insulating layer on the surface of the target causes arcing. In such a case, alumina deposits generally build up on the surface of the aluminum target causing an arc event. Arcing can adversely affect the structure and properties of the growing films. Therefore, when it is desirable to deposit such a film using a DC magnetron sputtering system, it is necessary to use a pulse-mode adapter for the DC power supply. This type of power supply has been found to prevent the formation of arcs at the target. <sup>25</sup>

### *3.1.5 PULSED MODE SPUTTER DEPOSITION*

Researchers have found that using medium frequency pulsed techniques can significantly overcome many disadvantages of magnetron

sputtering. Both the industrial and scientific research communities have used pulsed magnetron sputtering extensively. Using this technique, layers of aluminum oxide have been successfully deposited. This technique prevents the buildup of electrostatic charge on the insulating layers. The prevention of charge buildup serves to reduce or eliminate the occurrence of arcing events that cause surface defects. <sup>26</sup> Pulsed DC sputtering allows deposition of non-conductive materials with the magnetron system. In order to achieve the pulsed DC power we use a Sparc-le 20 power supply adapter. Advanced Energy manufactures the Sparc-le 20 power supply. This unit utilizes the original power supply, but it oscillates the original signal supplied to the guns.



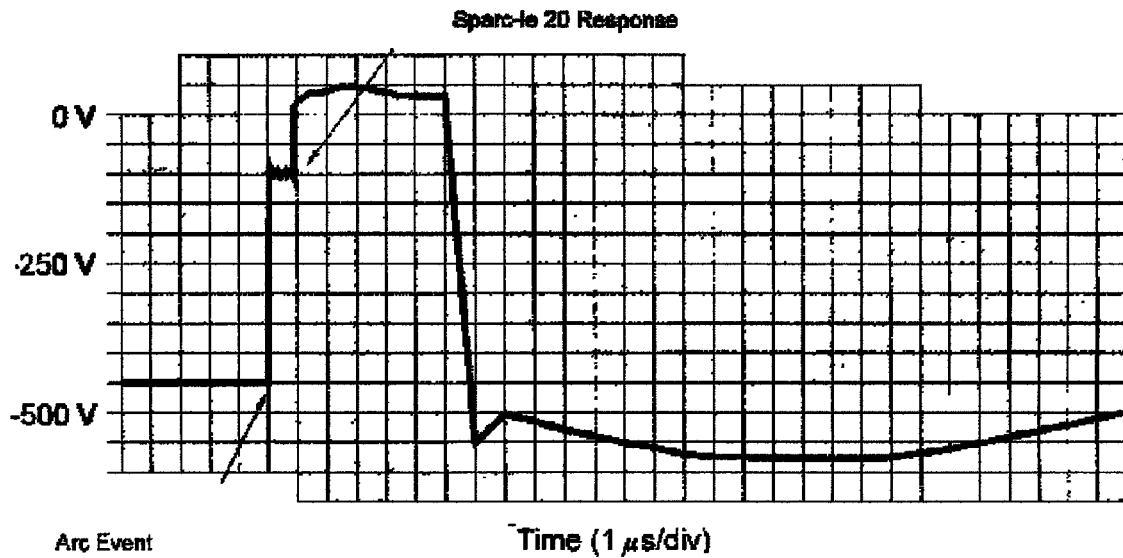
*Physical location of Sparc-le 20 in a system*

**Figure 10 - Schematic of Sparc-le 20 (courtesy of Advanced Energy)**

The figure above shows how the pulse unit operates in the system. Using the output of the MDX power supply as its input, the Sparc-le processes the signal and creates a pulsed output that is supplied to the guns. The Sparc-le 20 unit oscillates the DC bias at a frequency of 20 kHz. This pulse output helps to prevent charge buildup on the target and substrate. This unit has three main operating modes:

1. Self-Run
2. Arc-Out
3. Active-Arc

In self-run mode the Sparc-le 20 shorts out and reverses target voltage for 5 microseconds at a 20 kHz rate. In arc-out mode this unit functions only as a resonant LC network which discharges and then commutates off the arc through its reversing action. Our primary use of the Sparc-le 20 is running in active-arc mode. While operating in active arc-handling mode, the Sparc-le 20 can immediately shunt current away from the target when it detects the beginning of an arcing event. It is designed to respond to arcing events within microseconds. This process can be done at a rate of 40,000 arcs per second. The following illustration represents the Pulsed DC signal output of the Sparc-le 20 accessory. <sup>27</sup>



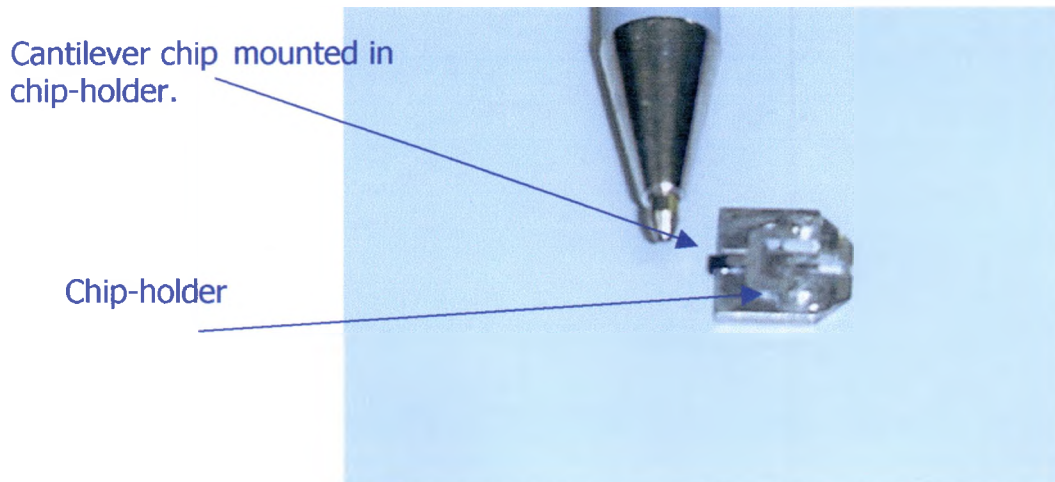
*Target voltage during active arc-handling mode*

Figure 11 - (courtesy of Advanced Energy)

## 3.2 SUBSTRATE MOUNTING

### 3.2.1 CANTILEVER CHIP HOLDER FOR SPUTTERING SYSTEM

One of the first obstacles we faced when trying to grow films on the cantilevers was the inability to position them in our process chamber. In order to sputter coat the cantilever chips we had to fabricate an experimental holder for them. This holder had to be vacuum compatible and have the ability to secure the tiny cantilever chips to the chamber without damaging them. Because of the small size of the cantilever chips, and since they are extremely fragile, care had to be taken in designing a suitable holder for them to be mounted in the chamber. The figure below illustrates the size of the cantilever chips with respect to an ordinary ballpoint pen.



**Figure 12 - Size comparison of AFM cantilever chip.**

### *3.2.2 MATERIAL SELECTION FOR CANTILEVER HOLDER*

Our holder design utilized machined stainless steel parts for vacuum compatibility. In order to sputter our AFM tips with the magnetron system we had to fabricate a device that could slide over the rectangular heater and still function as a delicate tip holder. By taking measurements from the tip holders that we already had we were able to come up with some specifications for our fabricated tip holder. The material chosen to construct the holder was non-magnetic stainless steel with a very fine polish. Brass and aluminum were also options. However, brass outgases if heated and aluminum would not endure high temperatures. Stainless steel is not a very porous metal, and with the polish on the surface it is compatible with our vacuum system. A porous metal can retain water and when in a vacuum it can “out-gas” causing an increase in the ultimate system pressure. The holder was constructed

in the department machine shop. The following diagrams and images illustrate the specifications of the fabricated tip holder.

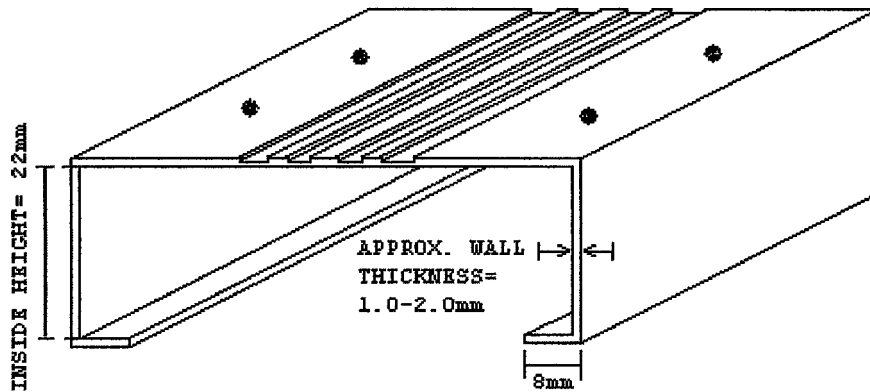


**Figure 13 - Diagram of cantilever holder.**

### **3.2.3 CANTILEVER HOLDER DESIGN**

One of the hardest processes in making the tip holder was to create the 0.25-mm channels in the hard stainless steel surface with a consistent depth along its length. This task was accomplished with a precision milling machine and a special 3.6-mm double-fluted bit. The multi-channel surface of the tip holder is a result of the adhesive properties of titanium. Since the metal sticks so well to just about anything, we did not want it to fill up the areas of the channel that were not being used. As sputtered material such as TiN is deposited it fills the channels. This material proves difficult to clean since it adheres so well to the substrate. Exposing only two channels at a time while covering the other two allowed us to ensure we were able to reuse the holder

device. The drawing below illustrates the critical dimensions of the channels.

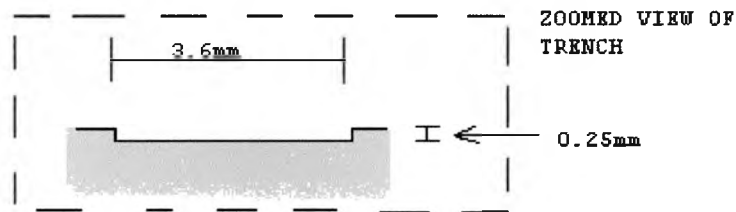


**Figure 14 - Dimensions of cantilever holder channels.**

### 3.2.4 SHUTTERS

Shutters also had to be constructed to fit on the holder in order to keep the cantilever chips from falling off the holder during the sputtering process and to shield part of the holder from the sputtered particles. Since the cantilever chips themselves are very fragile, the shutter design had to allow for delicate attachment of the cantilevers to the holder. In order to fasten the AFM tips to the holder the shutters had to have some flexibility. To this end we wrapped the center portions of the shutters with clean aluminum foil to cushion their grip on the cantilever chips. The shutters were fastened to the cantilever holder with stainless steel machine screws. Grooves were machined into the shutters to allow for adjustment when mounting the cantilever chips. These shutters were designed to accommodate the multiple channels in the tip holder as well as to be able to secure several cantilever chips to the holder at the same time. They are also used to prevent buildup of sputtered material on the

outer-most holder channels. The material used to make the shutters was the same used to fabricate the holder.

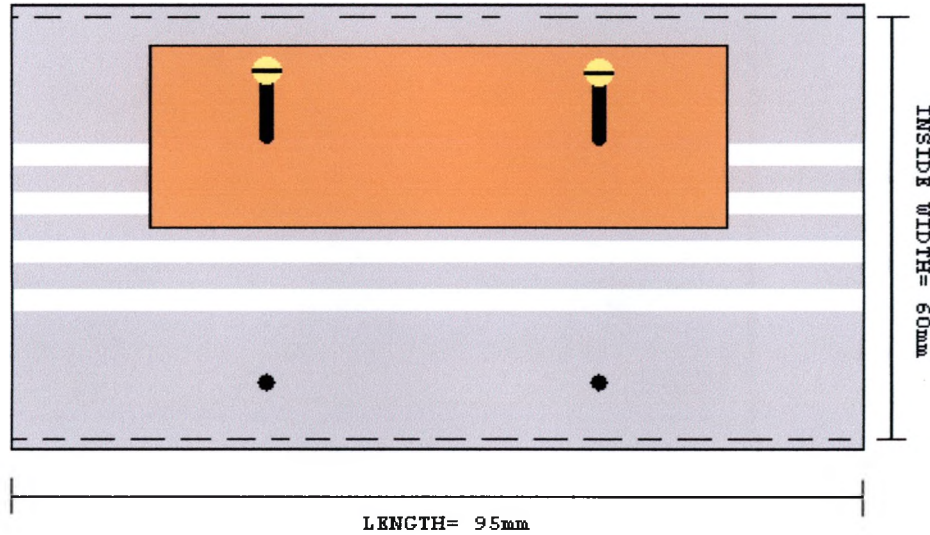


**Figure 15 - Top view of shutter.**

The purpose of the shutter is not only to fasten the cantilever to the holder assembly, but also to shield the rear channel from being deposited with titanium nitride. The titanium nitride deposits in the channels prevent the cantilever chips from being mounted flush to the surface of the holder. These deposits are also hard to clean and remove from the holder. Each side of the holder is equipped with its own shutter and they are designed to be easily moved/removed for loading and unloading tips. A cross sectional view of the shutter fastening the cantilever to the holder is given in the following illustration.

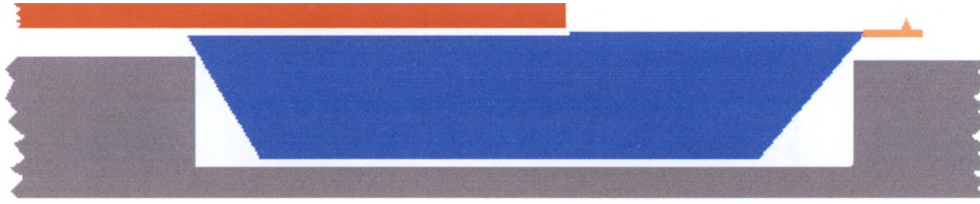


**Figure 16 – Cross-sectional view of cantilever chip mounted in holder.**

This illustration shows why the channel depth had to be no more than 0.25 mm. The cantilever chips are not much deeper than that, and if the channels were too deep the tips would break off before they were sputtered. The critical dimensions required for the cantilever holder made it difficult to machine using stainless steel as the material.

## CHAPTER 4

### Experimental Results and Modifications

#### 4.1 EQUIPMENT CALIBRATION

##### 4.1.1 CALIBRATION FILMS

The first step towards sputter coating the AFM cantilevers was to grow blanket films on 1.5 cm square substrates. These calibration films were needed because the size of the cantilevers would prevent us from directly measuring their material properties. The material properties of these blanket films were analyzed to determine the desired sputtering parameters to use for coating our tips. Our first attempt at sputter coating AFM cantilevers was made using the titanium nitride thin film on the capacitance imaging tips. A table of the initial sputtering parameters used for the first trial runs is given below.

Table 1 - List of sputtering parameters for calibration films.

Sample Number	Ar (sccm)	N2 (sccm)	Sput. time (s)	Power (W)	w/Ti seed (Y/N)	Heat
981217	6 0	2.0	500	200	Y (54s, 80W)	N
981230	6 0	2.0	600	200	N	N
981231	6 0	2.0	600	200	Y (60s, 80W)	N
990106	6.0	1 5	250	200	Y (60s, 50W)	N
990107	6.0	1 5	500	200	Y (60s, 50W)	N
990112	6.0	2 5	300	200	Y (60s, 50W)	N

## 4.2 PRELIMINARY RESULTS

### 4.2.1 ANALYSIS OF CALIBRATION FILMS

After the substrates were sputter coated, their individual thickness was measured. The film thickness enabled us to determine the growth rate of the deposition process. This information is also used in the resistivity calculations. Once the film thickness was measured the films were analyzed to determine their resistivity. The exact hardness of the sputtered films was not of extreme importance to us since we knew that titanium nitride was much more durable than the native silicon oxide tip. The resistivities of the initial blanket films were of the same order of magnitude that we would expect for bulk TiN. 14,15

**Table 2 - Film thickness and calculated resistivities.**

Sample Number	Thickness (Å)	Resistivity ( $\mu\Omega\text{-cm}$ )	Deposition Rate (Å/s)
981217	724	144.574	1.45
981230	899	233.692	1.50
981231	1137	176.457	1.90
990106	389	471.633	1.55
990107	1308	65.435	2.62
990112	454	178.503	1.51

### 4.2.2 SPUTTER COATING AFM CANTILEVERS

Since we were satisfied with our initial results, the same parameters were used in the tip coating process. After the cantilevers were coated they were removed from the holder and placed in a desiccator. Inspection of the coated cantilevers revealed a few visible

blemishes and deformities. Some of the cantilevers were destroyed during the sputter coating process. The surviving cantilevers were loaded into the AFM for testing.

#### 4.2.3 APPLICATION TESTING FOR LASER ALIGNMENT

Once the cantilevers are mounted in the AFM the first step is to align the laser on the middle-back of the tip. This is a relatively simple step and should not take long to complete. Once aligned, the laser should hit the middle-back of the cantilever and be reflected upwards to the Position-Sensitive Photo Diode (PSPD). This alignment is critical since the PSPD measures the amount of tips movement as the sample moves beneath the tip. The following image is an example of proper laser alignment.

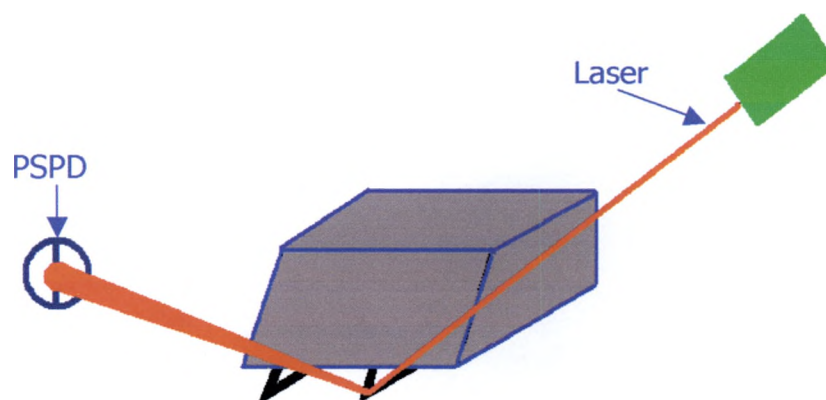
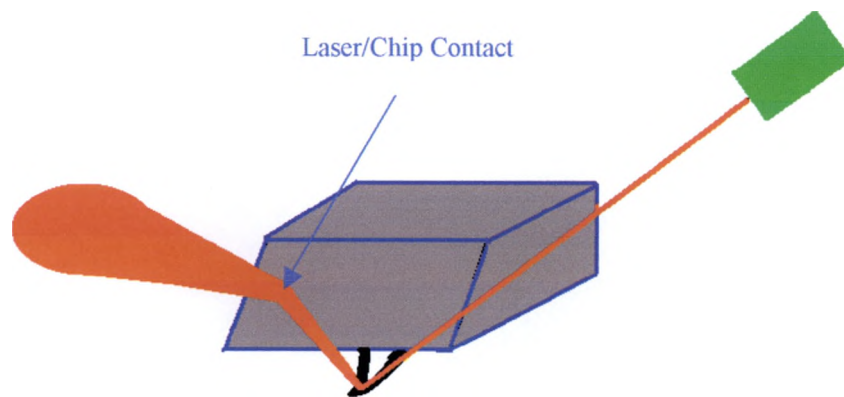


Figure 17 - Proper laser alignment on cantilever.

It was extremely difficult to achieve proper laser alignment with the newly coated cantilevers. Once the laser was centered on the back of the cantilever it was difficult to align on the PSPD. After several attempts at laser alignment the cantilever chip was removed for further inspection. Under a microscope the coated cantilevers seemed to be bent/curled in a fashion to prohibit proper alignment of the laser. The following figure illustrates the problem with the coated cantilevers.



**Figure 18 - Improper laser alignment.**

The laser, once centered on the back of the cantilever, was then reflected into the cantilever chip. Thus, the curled cantilevers made it nearly impossible to align the laser properly.

### **4.3 EXPERIMENTAL MODIFICATIONS**

#### *4.3.1 INTERFACIAL STRESS OF TITANIUM NITRIDE FILMS*

Since the majority of the cantilevers were unusable we began to investigate the cause of the deformities. The cantilevers themselves are very thin and fragile making them good stress detectors. The titanium nitride sticks so well to the silicon oxide cantilevers that the interfacial stress actually causes the cantilevers to bend. In our determination to use the TiN coatings we decided to use an adhesion layer of pure titanium in order to reduce the interfacial stress. This titanium seed layer is known to sometimes form a silicide on the surface of silicon. A titanium silicide layer would decrease the stress between the titanium nitride and the silicon interface.

#### *4.3.2 TITANIUM SEED LAYER*

Next we coated the cantilevers using the titanium seed layer beneath our titanium nitride coatings. This new process proved to be more effective than only using the TiN. After the sputtering process the cantilevers were visually inspected again revealing less deformation. Although many of the cantilevers seemed intact, there were still some cantilevers that were essentially destroyed. By increasing the thickness of the titanium seed layer we were able to further reduce the number of destroyed cantilevers. Using the surviving cantilevers we were able to properly align the laser on them and take some AFM capacitance images.

#### *4.3.3 DUAL TITANIUM TARGETS*

Although we were able to use some of the cantilevers that were coated using the titanium seed layer, we were still concerned with the small number of cantilevers that were destroyed during the sputtering process. Inspection of the titanium target used for sputtering yielded a visible nitride layer on its surface. This layer would make it nearly impossible to sputter a pure Ti seed layer. Initially, after sputtering a TiN layer in the chamber, we pre-sputtered the titanium target to remove any unwanted nitride deposits. This technique was used to prevent the deposition of TiN during the growth of the pure Ti seed layers. The pre-sputter was done with the shutters over the targets closed to prevent any film deposition on the samples. Since this technique did not seem to be working for us we tried a more reliable method. In order to ensure that we were getting a true titanium seed layer beneath the TiN layer we used dual titanium targets. One target was dedicated for the titanium growths and the other was dedicated for the titanium nitride growths. Since the design of our sputtering chamber enables us to use up to three different targets at the same time we did not have to break vacuum in order to use different targets.

## CHAPTER 5

### Film Analysis

#### 5.1 DEPOSITION RATES

##### 5.1.1 FILM THICKNESS

As mentioned earlier, the sputtered films were first analyzed to determine their resistivity. In order to calculate the resistivity of the thin films we first had to measure their thickness. When the square calibration films were grown in the sputtering chamber they were masked in order to provide a sharp step that could be measured to determine the thickness of the films. The following image represents the function of the mask on the substrate.

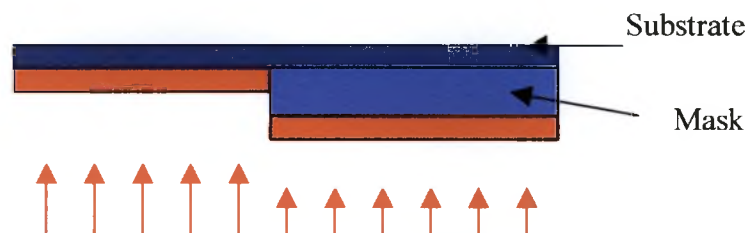
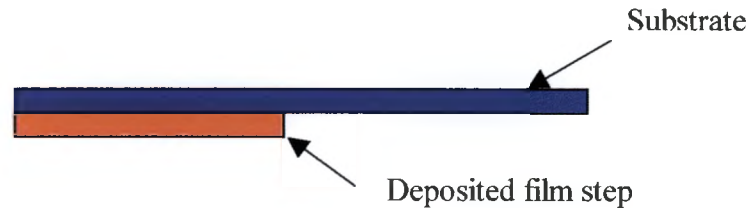


Figure 19 - Position of mask mounted on substrate during sputtering process.

This image illustrates how the sputtered material coats the substrate only in the areas not covered by the mask. When the samples are removed from the chamber the masks are also removed revealing the

step formed during the sputtering process. An illustration of the step created by the mask during the sputtering process is given below.



**Figure 20 - Step of sputtered material after mask removal.**

This step height was measured with a stylus profilometer. This instrument uses a diamond tip that is dragged across an area of the film that includes an abrupt step height contrasting the maximum height of the film and the substrate level (similar to a trench). The accuracy of the profilometer measurements is also important for determining proper deposition rates for each combination of sputtering parameters. Accurate deposition rates are required in order to achieve anticipated film thickness.

Another method used to mask the calibration films was to use two masks with a small spacing between them. This spacing allows the thin film to be deposited in a long narrow line on the surface of the substrate. If this line is made narrow enough (a few hundred nanometers) the profilometer can measure the “sep-up” on one side and the “step-down” on the other side of the film during a single scan. This method provides for a more accurate means of measuring the thickness of the films.

However, in order to get an accurate representation of the growth rate

the aspect ratio of the substrate features must not be too high. This ratio is the height of the masks divided by their separation. If the depth of the trench they form is larger than their separation then the sputtered molecules will not coat the step uniformly.

This method of masking can also be accomplished by drawing a line on the surface of the substrate with a non-permanent marker. This marker line prevents the sputtered film from adhering to the substrate where it is drawn. After sputtering is complete, the film can be removed where the line was drawn, revealing a trench similar to the previous method. This method usually forms steps that are not abrupt enough to be accurately measured with the profilometer.

### 5.1.2 TITANIUM/TITANIUM NITRIDE DEPOSITION RATES

The film thickness data from the titanium nitride calibration films was used to determine the sputter deposition rate of the TiN thin films. As mentioned above, these deposition rates were then used to estimate the proper sputtering time to achieve the desired film thickness when coating the AFM cantilevers.

**Table 3 - Deposition rates of various nitrogen gas flows.**

<b>Nitrogen Gas Flow (sccm)</b>	<b>Deposition Rate (Å/s)</b>
1.5	1.55
1.5	2.62
1.5	1.99
1.5	2.02
1.5	2.02

1.5	2.16
1.5	2.16
2.0	1.45
2.0	1.50
2.0	1.90

The table above represents growth rate for different nitrogen gas flows in the chamber when sputtering the titanium nitride calibration films. These growth rates were used to determine the amount of sputtering time needed to achieve thin films of desired thickness. The table below shows the mean deposition rate for each value of nitrogen gas flow from the preceding table as well as the standard deviation for each group of data.

**Table 4 - Mean deposition rates and standard deviation.**

<b>Nitrogen Gas Flow (sccm)</b>	<b>Mean Deposition Rate (A/s)</b>	<b><math>\sigma</math>Rate (A/s)</b>
1.5	2.06	0.31360688
2.0	1.61	0.24521653

The deposition rate of the titanium calibration films was more consistent since the only gas flow parameter was for the non-reactive argon gas. The flow rate of argon was kept constant (6.0 sccm) throughout the growth of both types of calibration films. The deposition rate for the pure titanium calibration films was around 1.0 angstroms/second.

### 5.1.3 ALUMINUM/ALUMINA DEPOSITION RATES

The data for aluminum oxide calibration films was used in a similar manner to determine the film thickness and then the deposition rate. The pure aluminum films were grown using the same constant argon flow of 6.0 sccm. These aluminum calibration films had a growth rate of about (1.2-1.5) angstroms/second. This deposition rate was used to estimate the time required to sputter the anticipated seed layer thickness on the AFM cantilevers.

The aluminum oxide thin films were grown using reactive sputtering of a pure aluminum target in an oxygen atmosphere. The oxygen flow rate was adjusted on the calibration films to determine the optimum value for alumina deposition. The chart below lists the deposition rates achieved with different oxygen flow rates for the alumina calibration films.

**Table 5 - Alumina deposition rates for different oxygen flows.**

<u>Sample Number</u>	<u>Argon Flow (sccm)</u>	<u>Oxygen Flow (sccm)</u>	<u>Deposition Rate (A/s)</u>
000208	6.0	1.50	4.61
000210	6.0	1.50	8.41
000223	6.0	1.25	7.56
000223	6.0	1.00	11.30

## 5.2 RESISTIVITY

### 5.2.1 FOUR-POINT-PROBE MEASUREMENTS

Once the thickness of the sputtered film is known this data can be used with four-point-probe (FPP) measurements to calculate the relative resistivity of the film. The FPP setup consists of four conducting test probes that are equally spaced and in-line with each other. These probes are brought into contact with the surface of the sample. A current is injected into the thin film through the two outer probes while at the same time the electric potential is measured over the two inner probes. In our case, the current is found by measuring the voltage drop across a known resistor as the current passes through it. This value is easily obtained since the current has a linear relationship with the measured voltage (i.e. Ohm's Law). The following equation is used to calculate the resistivity of the blanket films.

$$\rho = F_2 * t * (V/I)$$

The  $F_2$  factor in this equation is a constant of proportionality. It is representative of the probe and sample geometries. These geometries are also very important in achieving consistent data. This constant is needed to account for the fact that each sample is of slightly different sizes and shape. This factor is a function of the surface dimensions of the rectangular sputtered film and the probe spacing. In order to

determine the value of this constant, the dimensions were input into a Mathcad extrapolation program that was based on known factors for certain dimensions. The (V) in the above equation represents the voltage measured by the lock-in amplifier in the four-point-probe setup. The (I) in this equation represents the current flowing through the sample. This current is found by dividing the applied voltage by the value of a known resistor in the setup. The calculated resistivity allows us to compare the conductivity of the samples relative to each other. The table below lists some of the titanium nitride data describing the dimensions,  $F_2$  factor, and resistivity of the thin films. In this table, the (d/s) factor represents the film width divided by the film height. The four probes used in the FPP instrument run along the width of the film.

**Table 6 - Dimensions and resistivity of several titanium nitride thin films.**

<b>Sample Number</b>	<b>d/s</b>	<b>F2 Factor</b>	<b>Thickness (Å)</b>	<b>Resistivity (<math>\mu\Omega\text{-cm}</math>)</b>
<b>981217</b>	1.904	1.859	723.5	144.747
<b>981230</b>	1.8990	1.854	899.4	234.025
<b>981231</b>	1.965	1.914	1137.2	176.717
<b>990106</b>	1.718	1.689	388.7	472.437
<b>990107</b>	1.889	1.845	1307.8	65.480
<b>990112</b>	1.859	1.818	454.4	178.681
<b>990216 (full)</b>	3.778	2.968	1252.4	51.614
<b>990219 (full)</b>	3.778	2.968	1011	41.181
<b>990219 (half)</b>	1.874	1.832	1011	40.003

<b>990224 (full)</b>	3.778	2.968	1079.4	<b>37.820</b>
<b>990224 (half)</b>	1.955	1.905	1079.4	<b>37.121</b>

The consistency of the last several samples is apparent due to adjustments in the growth parameters of the films such as seed layer thickness, substrate temperature, pulsed-mode deposition, the use of dual Ti targets, and nitrogen flow. The specific parameters used for each growth can be found in the appendix.

The following table represents the data collected from two of the aluminum oxide film growths. This table lists the dimensions, F<sub>2</sub> factor, and resistivity of these alumina films.

**Table 7 - Dimensions and resistivity for aluminum oxide thin films.**

<b>Sample Number</b>	<b>d/s</b>	<b>F2 Factor</b>	<b>Thickness (Å)</b>	<b>Resistivity (<math>\mu\Omega\text{-cm}</math>)</b>
<b>000208-AI203</b>	3.778	2.968	2766.4	<b>2106.326</b>
<b>000216-AI203</b>	3.778	2.968	5043.2	<b>5806.751</b>

The data above indicates a large difference in the resistivity values for the two growths. The specific growth parameters, which have some effect on this data, can be found in the appendix. However, the fact that the resistivity values are so high indicates a highly insulating material. This is what we would expect to see from a material such as alumina,

which is now being used as a (high-k) gate dielectric material in the microelectronics manufacturing industry. 28,29

### 5.3 FILM UNIFORMITY AND ELEMENTAL ANALYSIS

#### 5.3.1 SEM AND EDS MAPPING

Another analytical tool used on the cantilevers was the scanning electron microscope (SEM). The SEM was used to image the actual tips themselves in order to determine the film uniformity with some degree of resolution. The SEM is also equipped with an Energy Dispersive Spectrometer (EDS).

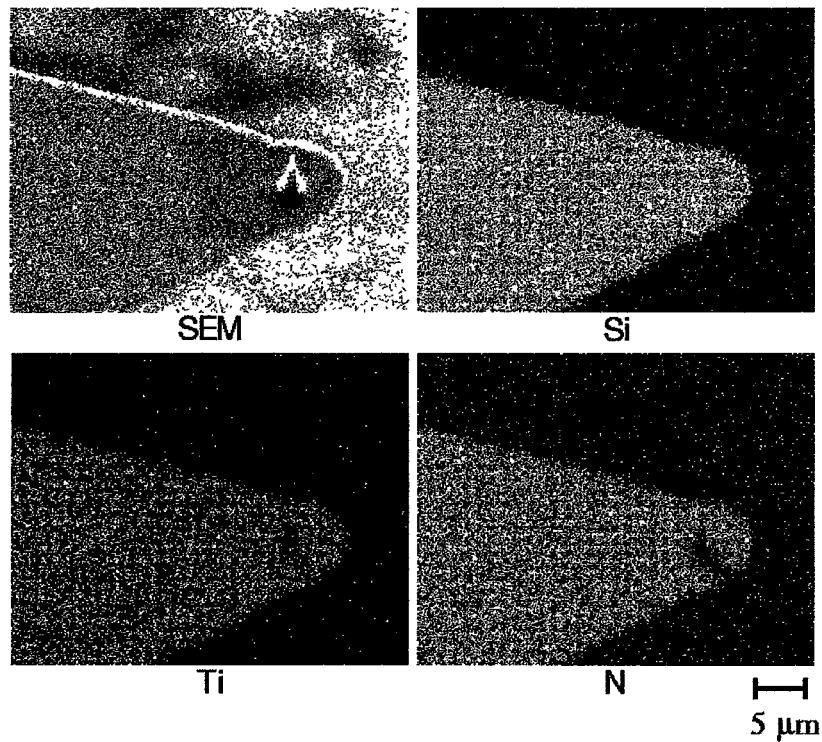


Figure 20 - EDS mapping of SEM image of AFM Ultralever.

This piece of equipment is used to determine the elemental composition of the SEM sample. With the help of Mike Matheaus the above images were taken with our SEM. The resolution of these images

is on the order of a micron. These EDS images show that, within the resolution of the image, there is titanium and nitrogen present at the apex of the cantilever where the tip is located. These images also give some insight as to the ultimate film uniformity across the entire cantilever.

## **5.4 ELECTRICAL PROPERTIES OF TITANIUM NITRIDE**

### *5.4.1 CONDUCTIVITY*

In order to show that the TiN coated cantilevers were more conductive than the original silicon oxide cantilevers we acquired I-V spectra of the different tips. Similar to the Four-Point-Probe apparatus, we applied a bias between the tip and sample and measured the current traveling between them. This current is plotted against the voltage in the following figure. In this figure we can see the difference in conductivity between the conductive TiN coated cantilevers and the silicon oxide cantilevers. The curve of the lines is representative of a semiconductor. This is likely since the cantilever tip is actually made of silicon. The larger slope for the coated cantilever tip is representative of a material with higher conductivity. This slope means that more current can flow with less applied voltage than the non-conductive tip.

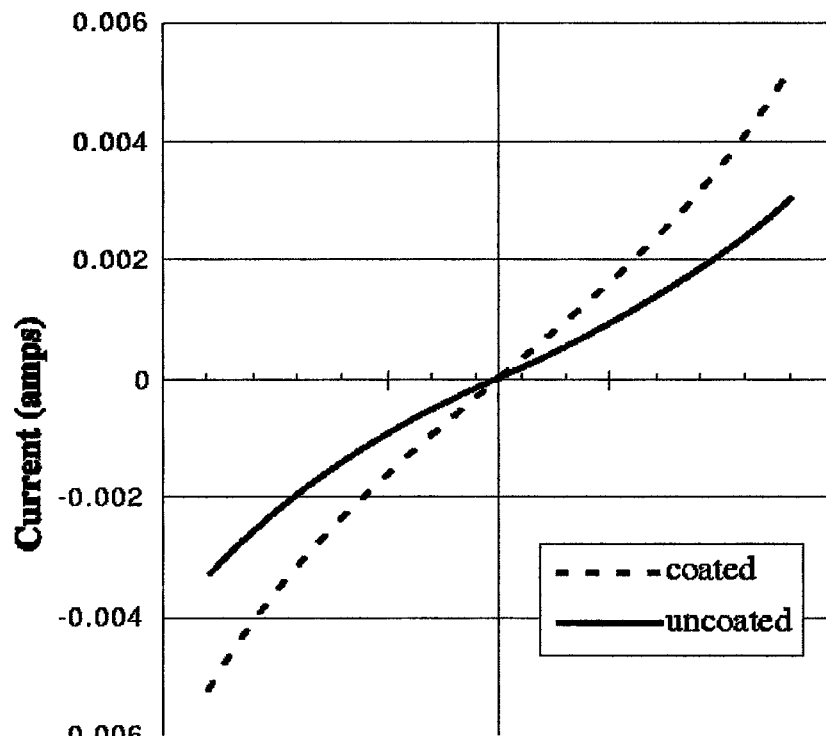


Figure 22 - (I vs. V) plot of coated and uncoated AFM Ultralever.

## **CHAPTER 6**

### **Conclusions**

#### **6.1 CONCLUSIONS**

One of the most important pieces of equipment that we use in our lab for materials research is the Atomic Force Microscope. This instrument is used in a variety of ways to examine the atomic-scale physical properties of materials. We have used our AFM for capacitance imaging and chemical mechanical planarization (CMP) modeling. Capacitance imaging allows us to effectively image the local dielectric properties of materials. By modeling atomic scale CMP we can gain insight to some of the fundamental mechanisms. Operating this instrument in these ways requires the use of specialized cantilever tips. For our capacitance imaging we fabricated a tip that is both durable and conductive by coating the standard silicon oxide AFM cantilevers with titanium nitride. Cantilevers were also fabricated for our atomic-scale CMP modeling application using certain specialized materials such as aluminum oxide. By sputter-coating generic “store-bought” tips, we have fabricated our own tips for various applications. This process was done using our DC Magnetron Sputtering System. Selected films have been grown in this system that meet our requirements for our various AFM

applications. In order to reliably coat tips for our research applications, we determined the type of material that was best suited for our application. Next, we experimentally determined the ideal recipe for growing the desired films. To do this, blanket films are grown on sample substrates and then analyzed to determine their physical properties. Once a recipe was generated, a reliable/repeatable system for mounting the fragile cantilever chips in the sputtering chamber was developed. The AFM cantilever chips were mounted in the sputtering chamber using a specially designed and machined tip holder. Using the tip holder I designed I have been able to successfully sputter-coat the AFM cantilevers. After the cantilever chips were coated, they were analyzed in order to determine their physical properties. From this research we have shown that is possible for small research groups to effectively and cost-consciously sputter-coat microfabricated AFM cantilevers for specific research applications.

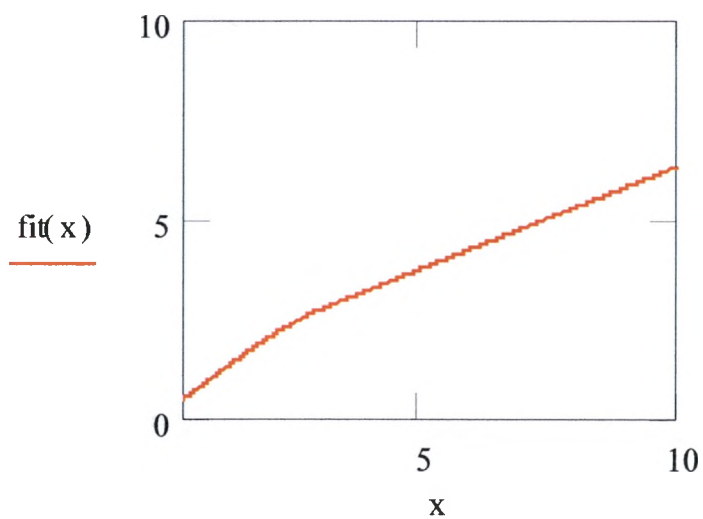
**APPENDIX**

The following equations and charts in this section of the appendix are from the Mathcad program used to determine the  $F_2$  factor in the resistivity calculations using the four-point-probe apparatus.

**FOR a/d=2**

$$X := \begin{bmatrix} 1.5 \\ 1.75 \\ 2 \\ 2.5 \\ 3 \\ 4 \end{bmatrix} \quad Y := \begin{bmatrix} 1.4788 \\ 1.7196 \\ 1.9454 \\ 2.3532 \\ 2.7 \\ 3.2246 \end{bmatrix}$$

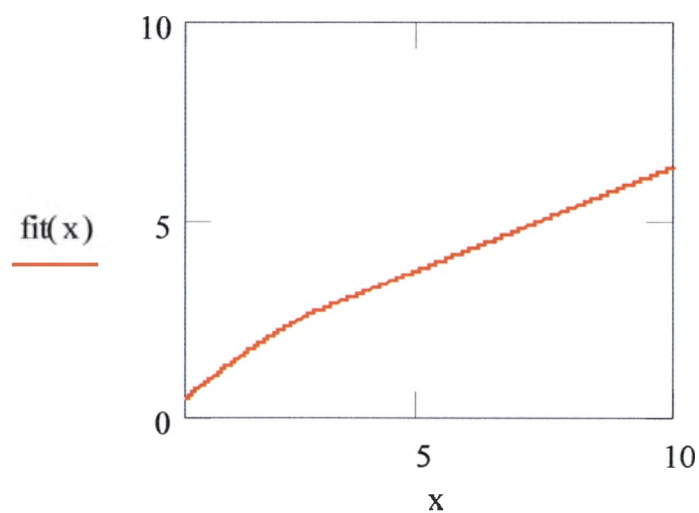
$$\text{fit}(x) := \text{linterp}(X, Y, x) \quad \text{fit}(3) = 2.7$$



**FOR a/d=3**

$X :=$	1	$Y :=$	.9988
	1.25		1.2467
	1.5		1.4893
	1.75		1.7238
	2		1.9475
	2.5		2.3541
	3		2.7005
	4		3.2248

$$\text{fit}(x) := \text{linterp}(X, Y, x) \quad \text{fit}(3) = 2.7$$



These charts are created from interpolated data and used to determine an accurate value for the  $F_2$  factor used in the resistivity measurements. The  $d/s$  values are obtained by direct measurement of the substrate dimensions.

The follow tables and charts represent the raw data taken while performing the four-point-probe resistivity measurements.

<b>SAMPLE</b>	<b>Vpp(applied)</b>	<b>V(lock-in)</b>	<b>Thickness (Å)</b>	<b>a (cm)</b>	<b>d (cm)</b>
<b>981217</b>	1.00	17.33	723.5	1.5	0.7
	1.50	25.99			
	2.00	34.60			
	2.50	43.27			
	3.00	51.90			
	3.50	60.52			
<b>981230</b>	1.00	22.60	899.4	1.5	0.75
	1.50	33.90			
	2.00	45.10			
	2.50	56.41			
	3.00	67.65			
	3.50	78.90			
<b>990106</b>	1.00	115.88	388.67	1.5	0.7
	1.50	173.74			
	2.00	231.10			
	2.50	289.10			
	3.00	346.80			
	3.50	404.60			
<b>990107</b>	1.00	4.37	1307.8	1.5	0.75
	1.50	6.56			
	2.00	8.73			
	2.50	10.91			
	3.00	13.10			
	3.50	15.27			
<b>990112</b>	1.00	34.83	1137.2	1.5	0.75
	1.50	52.25			
	2.00	69.55			
	2.50	87.02			
	3.00	104.29			
	3.50	121.67			

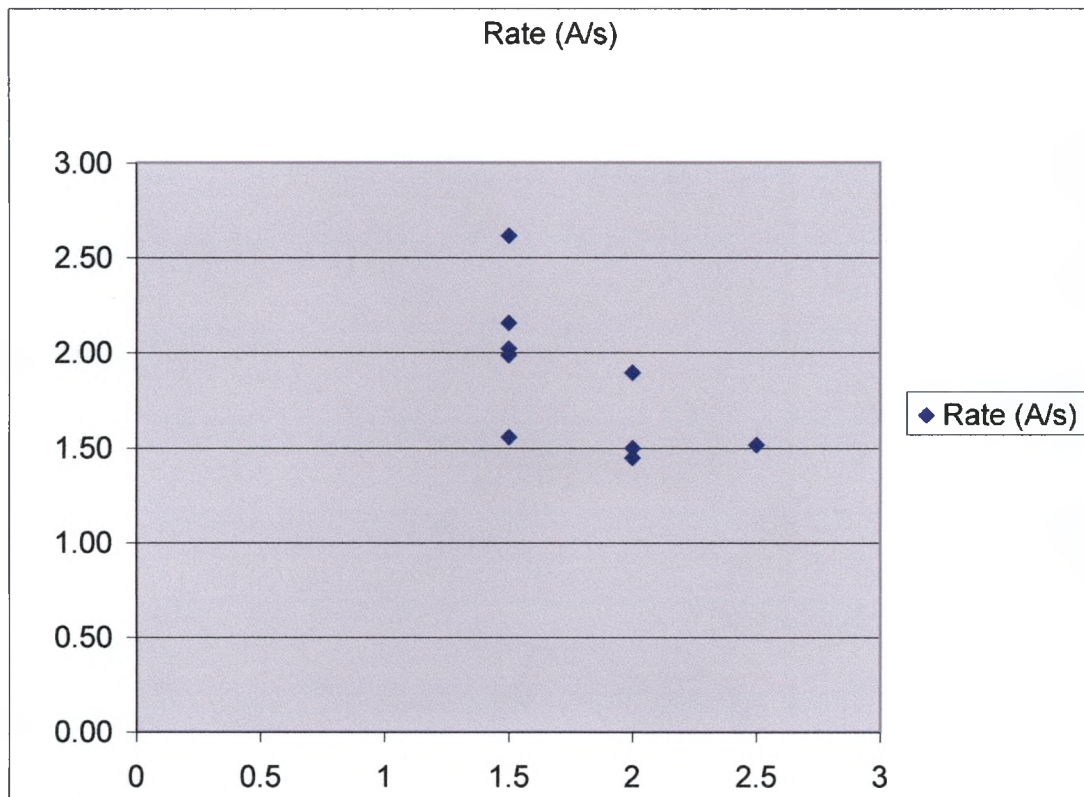
The next table lists some important film growth parameters as well as the measured thickness, calculated resistivity, and deposition rate.

<u>Sample Number</u>	<u>Ar (sccm)</u>	<u>N2 (sccm)</u>	<u>Sput. time (s)</u>	<u>Power (W)</u>	<u>Thickness (Å)</u>	<u>w/Ti seed (Y/N)</u>	<u>Resistivity (<math>\mu\Omega\text{-cm}</math>)</u>	<u>Heat</u>	<u>Rate (Å/s)</u>
981217	6.0	2.0	500	200	724	Y (54s, 80W)	144.574	N	1.45
981230	6.0	2.0	600	200	899	N	233.692	N	1.50
981231	6.0	2.0	600	200	1137	Y (60s, 80W)	176.457	N	1.90
990106	6.0	1.5	250	200	389	Y (60s, 50W)	471.633	N	1.55
990107	6.0	1.5	500	200	1308	Y (60s, 50W)	65.435	N	2.62
990112	6.0	2.5	300	200	454	Y (60s, 50W)	178.503	N	1.51
990216 (full)	6.0	1.5	630	200	1252	Y (60s, 50W)	51.536	300 (C)	1.99
990219 (full)	6.0	1.5	500	200	1011	Y (60s, 50W)	41.126	346 (C)	2.02
990219 (half)	6.0	1.5	500	200	1011	Y (60s, 50W)	39.956	346 (C)	2.02
990224 (full)	6.0	1.5	500	200	1079	Y (60s, 50W)	37.774	396 (C)	2.16
990224 (half)	6.0	1.5	500	200	1079	Y (60s, 50W)	37.082	396 (C)	2.16
990514	6.0	1.5	500	200	762.2	Y (90s, 50W, 200 C)	99.893	350 (C)	1.45

The table below lists the different growth rates achieved while varying the gas flow parameter.

<u>N2 (sccm)</u>	<u>Rate (Å/s)</u>	<u>N2 (sccm)</u>	<u>Rate (Å/s)</u>	<u><math>\sigma</math>Rate (Å/s)</u>
1.5	1.55	1.5	2.06	0.314
1.5	2.62	2.0	1.61	0.245
1.5	1.99	2.5	1.51	N/A
1.5	2.02			
1.5	2.02			
1.5	2.16			
1.5	2.16			
2.0	1.45			
2.0	1.50			
2.0	1.90			
2.5	1.51			

The following chart represents the plotted growth rate data collected while varying the gas flow during the sputtering process.



The table below is a complete list of the acquired and calculated data relating to the resistivity of the sputtered thin film growths.

<b>Sample Number</b>	<b>Applied Voltage (V)</b>	<b>Lock-in Voltage (mV)</b>	<b>Current (A)</b>	<b>d/s</b>	<b>F2 Factor</b>	<b>Thickness (Å)</b>	<b>Resistivity (<math>\mu\Omega\text{-cm}</math>)</b>
R= 621 ohms s= 0.397 cm							
<b>981217</b>	1.0	17.33	0.001610306	1.904	1.859	723.5	144.747
	1.5	25.99	0.002415459	1.904	1.859	723.5	144.719
	2.0	34.60	0.003220612	1.904	1.859	723.5	144.496
	2.5	43.27	0.004025765	1.904	1.859	723.5	144.563
	3.0	51.90	0.004830918	1.904	1.859	723.5	144.496
	3.5	60.52	0.005636071	1.904	1.859	723.5	144.424
						mean	144.574
<b>981230</b>	1.0	22.60	0.001610306	1.8990	1.854	899.4	234.025
	1.5	33.90	0.002415459	1.8990	1.854	899.4	234.025
	2.0	45.10	0.003220612	1.8990	1.854	899.4	233.507
	2.5	56.41	0.004025765	1.8990	1.854	899.4	233.652
	3.0	67.65	0.004830918	1.8990	1.854	899.4	233.507
	3.5	78.90	0.005636071	1.8990	1.854	899.4	233.433
						mean	233.692
<b>981231</b>	1.0	13.07	0.001610306	1.965	1.914	1137.2	176.717
	1.5	19.61	0.002415459	1.965	1.914	1137.2	176.672
	2.0	26.09	0.003220612	1.965	1.914	1137.2	176.325
	2.5	32.63	0.004025765	1.965	1.914	1137.2	176.420
	3.0	39.14	0.004830918	1.965	1.914	1137.2	176.348
	3.5	45.64	0.005636071	1.965	1.914	1137.2	176.258
						mean	176.457
<b>990106</b>	1.0	115.88	0.001610306	1.718	1.689	388.7	472.437
	1.5	173.74	0.002415459	1.718	1.689	388.7	472.220
	2.0	231.10	0.003220612	1.718	1.689	388.7	471.092
	2.5	289.10	0.004025765	1.718	1.689	388.7	471.459
	3.0	346.80	0.004830918	1.718	1.689	388.7	471.296
	3.5	404.60	0.005636071	1.718	1.689	388.7	471.296
						mean	471.633
<b>990107</b>	1.0	4.37	0.001610306	1.889	1.845	1307.8	65.480
	1.5	6.56	0.002415459	1.889	1.845	1307.8	65.530
	2.0	8.73	0.003220612	1.889	1.845	1307.8	65.405
	2.5	10.91	0.004025765	1.889	1.845	1307.8	65.390
	3.0	13.10	0.004830918	1.889	1.845	1307.8	65.430

	3.5	15.27	0.005636071	1.889	1.845	1307.8	65.373
						mean	65.435
<b>990112</b>	1.0	34.83	0.001610306	1.859	1.818	454.4	178.681
	1.5	52.25	0.002415459	1.859	1.818	454.4	178.698
	2.0	69.55	0.003220612	1.859	1.818	454.4	178.398
	2.5	87.02	0.004025765	1.859	1.818	454.4	178.568
	3.0	104.29	0.004830918	1.859	1.818	454.4	178.339
	3.5	121.67	0.005636071	1.859	1.818	454.4	178.336
						mean	178.503
<b>990216 (full)</b>	1.0	2.24	0.001610306	3.778	2.968	1252.4	51.614
	1.5	3.35	0.002415459	3.778	2.968	1252.4	51.599
	2.0	4.46	0.003220612	3.778	2.968	1252.4	51.499
	2.5	5.58	0.004025765	3.778	2.968	1252.4	51.540
	3.0	6.69	0.004830918	3.778	2.968	1252.4	51.491
	3.5	7.80	0.005636071	3.778	2.968	1252.4	51.469
						mean	51.536
<b>990219 (full)</b>	1.0	2.21	0.001610306	3.778	2.968	1011	41.181
	1.5	3.32	0.002415459	3.778	2.968	1011	41.181
	2.0	4.41	0.003220612	3.778	2.968	1011	41.097
	2.5	5.52	0.004025765	3.778	2.968	1011	41.122
	3.0	6.62	0.004830918	3.778	2.968	1011	41.094
	3.5	7.72	0.005636071	3.778	2.968	1011	41.080
						mean	41.126
<b>990219 (half)</b>	1.0	3.48	0.001610306	1.874	1.832	1011	40.003
	1.5	5.22	0.002415459	1.874	1.832	1011	40.003
	2.0	6.94	0.003220612	1.874	1.832	1011	39.923
	2.5	8.68	0.004025765	1.874	1.832	1011	39.948
	3.0	10.42	0.004830918	1.874	1.832	1011	39.934
	3.5	12.15	0.005636071	1.874	1.832	1011	39.925
						mean	39.956
<b>990224 (full)</b>	1.0	1.90	0.001610306	3.778	2.968	1079.4	37.820
	1.5	2.85	0.002415459	3.778	2.968	1079.4	37.827
	2.0	3.80	0.003220612	3.778	2.968	1079.4	37.750
	2.5	4.75	0.004025765	3.778	2.968	1079.4	37.768
	3.0	5.69	0.004830918	3.778	2.968	1079.4	37.747
	3.5	6.64	0.005636071	3.778	2.968	1079.4	37.732
						mean	37.774
<b>990224 (half)</b>	1.0	2.91	0.001610306	1.955	1.905	1079.4	37.121
	1.5	4.36	0.002415459	1.955	1.905	1079.4	37.125
	2.0	5.80	0.003220612	1.955	1.905	1079.4	37.050

	2.5	7.26	0.004025765	1.955	1.905	1079.4	37.077
	3.0	8.71	0.004830918	1.955	1.905	1079.4	37.057
	3.5	10.16	0.005636071	1.955	1.905	1079.4	37.064
						mean	37.082
<b>990514 (full)</b>	1.0	7.12	0.001610306	3.778	2.968	762.2	100.038
	1.5	10.68	0.002415459	3.778	2.968	762.2	100.005
	2.0	14.21	0.003220612	3.778	2.968	762.2	99.841
	2.5	17.78	0.004025765	3.778	2.968	762.2	99.900
	3.0	21.31	0.004830918	3.778	2.968	762.2	99.790
	3.5	24.86	0.005636071	3.778	2.968	762.2	99.783
						mean	99.893
<b>990518 (full)</b>	1.0	3.96	0.001610306	3.778	2.968	738.2	53.920
	1.5	5.94	0.002415459	3.778	2.968	738.2	53.916
	2.0	7.91	0.003220612	3.778	2.968	738.2	53.805
	2.5	9.89	0.004025765	3.778	2.968	738.2	53.847
	3.0	11.86	0.004830918	3.778	2.968	738.2	53.807
	3.5	13.84	0.005636071	3.778	2.968	738.2	53.790
						mean	53.848
<b>000208-AI</b>	1.0	0.2698	0.001610306	3.778	2.968	752.6	3.742
	1.5	0.4048	0.002415459	3.778	2.968	752.6	3.743
	2.0	0.5388	0.003220612	3.778	2.968	752.6	3.737
	2.5	0.6743	0.004025765	3.778	2.968	752.6	3.741
	3.0	0.8087	0.004830918	3.778	2.968	752.6	3.739
	3.5	0.9435	0.005636071	3.778	2.968	752.6	3.739
						mean	3.740
<b>000208-AI203</b>	1.0	41.31	0.001610306	3.778	2.968	2766.4	2106.326
	1.5	61.97	0.002415459	3.778	2.968	2766.4	2106.496
	2.0	82.47	0.003220612	3.778	2.968	2766.4	2102.502
	2.5	103.10	0.004025765	3.778	2.968	2766.4	2102.757
	3.0	123.63	0.004830918	3.778	2.968	2766.4	2101.228
	3.5	144.20	0.005636071	3.778	2.968	2766.4	2100.718
						mean	2103.338
<b>000209-AI</b>	1.0	0.3138	0.001610306	3.778	2.968	871.6	5.041
	1.5	0.4710	0.002415459	3.778	2.968	871.6	5.044
	2.0	0.6270	0.003220612	3.778	2.968	871.6	5.036
	2.5	0.7840	0.004025765	3.778	2.968	871.6	5.038
	3.0	0.9410	0.004830918	3.778	2.968	871.6	5.039
	3.5	1.0980	0.005636071	3.778	2.968	871.6	5.040
						mean	5.040
<b>000209-AI203</b>	1.0	1.252	0.001610306	3.778	2.968	103.7	2.393

	1.5	1.879	0.002415459	3.778	2.968	103.7	2.394
	2.0	2.500	0.003220612	3.778	2.968	103.7	2.389
	2.5	3.128	0.004025765	3.778	2.968	103.7	2.391
	3.0	3.751	0.004830918	3.778	2.968	103.7	2.390
	3.5	4.377	0.005636071	3.778	2.968	103.7	2.390
						mean	2.391
<b>000210-AI-100W</b>	1.0	0.2890	0.001610306	3.778	2.968	777.75	4.143
	1.5	0.4337	0.002415459	3.778	2.968	777.75	4.145
	2.0	0.5770	0.003220612	3.778	2.968	777.75	4.136
	2.5	0.7220	0.004025765	3.778	2.968	777.75	4.140
	3.0	0.8660	0.004830918	3.778	2.968	777.75	4.138
	3.5	1.0100	0.005636071	3.778	2.968	777.75	4.137
						mean	4.140
<b>000210-AI-150W</b>	1.0	0.1729	0.001610306	3.778	2.968	995	3.171
	1.5	0.2597	0.002415459	3.778	2.968	995	3.175
	2.0	0.3457	0.003220612	3.778	2.968	995	3.170
	2.5	0.4324	0.004025765	3.778	2.968	995	3.172
	3.0	0.5190	0.004830918	3.778	2.968	995	3.173
	3.5	0.6047	0.005636071	3.778	2.968	995	3.168
						mean	3.171
<b>000216-AI203</b>	1.0	62.47	0.001610306	3.778	2.968	5043.2	5806.751
	1.5	93.73	0.002415459	3.778	2.968	5043.2	5808.300
	2.0	124.86	0.003220612	3.778	2.968	5043.2	5803.033
	2.5	156.36	0.004025765	3.778	2.968	5043.2	5813.629
	3.0	187.70	0.004830918	3.778	2.968	5043.2	5815.736
	3.5	219.10	0.005636071	3.778	2.968	5043.2	5818.835
						mean	5811.047

**BIBLIOGRAPHY**

- <sup>1</sup>Robert W. Carpick and Miquel Salmeron, "Scratching the Surface: Fundamental Investigations of Tribology with Atomic Force Microscopy," *Chemical Reviews* **97** (4), 1163-1194 (1997).
- <sup>2</sup>Steven M. Hues, Richard J. Colton, Ernst Meyer *et al.*, "Scanning Probe Microscopy of Thin Films," *MRS Bulletin* (January), 41-42 (1993).
- <sup>3</sup>C.F. Quate, "The AFM as a Tool for Surface Imaging," *Surface Science*, 980 (1994).
- <sup>4</sup>G. Binnig, C.F. Quate, and Ch. Gerber, "Atomic Force Microscope," *Physical Review Letters* **56** (9), 930-932 (1986).
- <sup>5</sup>C.Y. Chang and S.M. Sze, *ULSI Technology* (McGraw-Hill, Singapore, 1996).
- <sup>6</sup>S. Hudlet, M. Saint Jean, B. Roulet *et al.*, "Electrostatic Forces Between Metallic Tip and Semiconductor Surface," *Journal of Applied Physics* **77** (7), 3308-3313 (1995).
- <sup>7</sup>Y. Huang and C.C. Williams, "Direct Comparison of Cross-Sectional Scanning Capacitance Microscope Dopant Profile and Vertical Ion-Mass Spectroscopy Profile," *JVST B* **14** (1), 433 (1996).
- <sup>8</sup>Kazuya Goto and Kazuhiro Hane, "Tapping Mode Capacitance Microscopy," *Rev. Sci. Instrum.* **68** (1), 120 (1997).

- <sup>9</sup>S. Lanyi, J. Torok, and P. Reherek, "Imaging Conducting Surfaces of Dielectric Films by Scanning Capacitance Microscope," *Journal of Vacuum Science and Technology B* **14** (2), 892 (1996).
- <sup>10</sup>J.J. Kopanski and S. Mayo, "Intermittent-Contact Scanning Capacitance Microscope for Lithographic Overlay Measurement," *Applied Physics Letters* **72** (19), 2469 (1998).
- <sup>11</sup>Yale Strausser and Dale L. Hetherington, "AFM Measurements in Support of CMP.," (Digital Instruments, 1996), Vol. 2000.
- <sup>12</sup>Inc. Advanced Surface Microscopy, "Atomic Force Microscopy," (2000), Vol. 2000.
- <sup>13</sup>D. Devecchio, P. Schmutz, and G. S. Frankel, "A New Approach for the Study of Chemical Mechanical Polishing," *Electrochemical and Solid-State Letters* **3** (2), 90-92 (2000).
- <sup>14</sup>D. S. Williams, F. A. Baiocchi, R. C. Beirsto *et al.*, "Nitrogen, Oxygen, and Argon Incorporation During Rective Sputter Deposition of Titanium Nitride," *JVST* (1987).
- <sup>15</sup>D. Maheo and J. M. Poitevin, "Microstructure and Electrical Resistivity of TiN Films Deposited on Heated and Negatively Biased Silicon Substrates," *Thin Solid Films* **237**, 78 (1994).
- <sup>16</sup>Kenji Hinode, Yoshio Homma, and Mitsuaki Hriuchi, "Morphology-Dependent Oxidation Behavior of Reactively Sputtered Titanium-Nitride Films," *JVST A* **15** (4), 2017 (1997).

- <sup>17</sup>S.J. O'Shea, R.M. Atta, and M.E. Welland, "Characterization of Tips for Conducting Atomic Force Microscopy," *Rev. Sci. Instrum.* **66** (3), 2508-2512 (1995).
- <sup>18</sup>Hirofumi Sumi, Hajime Inoue, Yukiyasu Sugano *et al.*, "Characterizations of TiN Films Sputter under Optimized Conditions of Metallic Mode Deposition," *Journal of Applied Physics* **36** (2), 595 (1997).
- <sup>19</sup>Materials Research Corporation, *The Basics of Sputtering*, Third ed. (MRC, 1980).
- <sup>20</sup>W. R. Runyan and K. E. Bean, "Deposition of Inorganoc Thin Films," in *Semiconductor Integrated Circuit Processing Technology* (Addison-Wesley, New York, 1992), pp. 124.
- <sup>21</sup>L. Hultman, J. E. Sundgren, L. C. Markert *et al.*, "Ar And Excess N Incorporation in Epitaxial TiN Films Grown By Reactive Bias Sputtering in Mixed Ar/N<sub>2</sub> and Pure Ns Discharges," *JVST* (1989).
- <sup>22</sup>Emilio Martines, "DC Magnetron Sputtering Plasmas," (2000).
- <sup>23</sup>Vic Comello, "Sputtering, the Versatile Coating Process," in *R&D Magazine* (1998), Vol. May, pp. 71.
- <sup>24</sup>F. Elstner, A. Ehrlich, H. Kupfer *et al.*, "Structure and Properties of Titanium Nitride Thin Films Deposited at Low Temperatures Using Direct Current Magnetron Sputtering," *JVST A* **21** (2), 476 (1994).
- <sup>25</sup>P. J. Kelly and R. D. Arnell, "Control of the structure and properties of aluminum oxide coatings deposited by pulsed magnetron sputtering,"

Journal of Vacuum Science & Technology A (Vacuum, Surfaces, and Films) **17** (3), 945-53 (1999).

<sup>26</sup>Inc. Huettinger Electronics, "Pulsed Magnetron Sputtering," (1996-1997), Vol. 2000.

<sup>27</sup>Advanced Energy, "User Manual," in *Advanced Energy MDX Sparc-le 20* (Advanced Energy, Fort Collins, 1998).

<sup>28</sup>T. M. Klein, D. Niu, W. S. Epling *et al.*, "Evidence of Aluminum Silicate Formation during Chemical Vapor Deposition of Amorphous Al<sub>2</sub>O<sub>3</sub> Thin Films on Si(100)," *Applied Physics Letters* **75** (25), 4001 (1999).

<sup>29</sup>E. P. Gusev, M. Copel, E. Cartier *et al.*, "High-Resolution Depth Profiling in Ultrathin Al<sub>2</sub>O<sub>3</sub> Films on Si," *Applied Physics Letters* **76** (2), 176 (2000).



